

## MINERALOGY OF LEUCITE-BEARING DYKES FROM NAPOLEON BAY, BAFFIN ISLAND: MULTISTAGE PROTEROZOIC LAMPROITES

DONALD D. HOGARTH

Department of Geology, University of Ottawa, Ottawa, Ontario K1N 6N5

### ABSTRACT

Vertical, W- and NW-trending, post-tectonic, Proterozoic dykes at Napoleon Bay, southeastern Baffin Island, Northwest Territories, contain mineral assemblages typical of lamproites: 1) phenocrysts of Fe-bearing leucite and sanidine, Ti-rich phlogopite, and high-Mg olivine and diopside, and 2) a groundmass of Ti-rich phlogopite, Fe-bearing sanidine and apatite. Except where preserved in chill zones, leucite has decomposed to a sanidine – kalsilite intergrowth or has been replaced completely by sanidine. Phlogopite grains are enriched in Fe (to annite and ferri-annite) on their margins, relative to cores. Late-stage titanian potassium magnesio-arfvedsonite appears in some dykes and is also progressively enriched in Fe (to titanian potassium arfvedsonite) toward the margins of grains. In a few crystals, aegirine and aegirine-augite (some grains Ti-rich) overgrow diopside. Rare and very late-stage, possibly magmatic development of minerals involves overgrowths of potassium magnesio-arfvedsonite on Fe-rich amphibole, and phlogopite and “ferriphlogopite” on Fe-rich mica. With the exception of aegirine and aegirine-augite, all ferromagnesian silicates are undersaturated in  $\text{Si} + \text{IVAl}$ , with average deficits in the tetrahedral position extending from 15.7% in annite and ferri-annite (grain margins) to 1.5% in magnesio-arfvedsonite (overgrowths). The vacancies in the tetrahedral position can be filled with  $\text{Fe}^{3+}$ . Rare minerals in the Baffin dykes, that are characteristic of known occurrences of lamproite, are K, Ti-rich sodic-calcic amphiboles, shcherbakovite, Ti-rich chromite, and K-Ti-Fe oxide. However, some minor minerals in these dykes have not been described from lamproite [pectolite, lorenzenite, barytolamprophyllite, calcioancylite-(Ce), djerfisherite], and the late Na-Fe overprint seems extreme for lamproite. Evidence suggests differentiation with repeated, post-consolidation magmatic injections. Rocks that are possibly related include a porphyritic volcanic rock containing pseudoleucite (sanidine) – forsterite – diopside – titanian phlogopite, located ca. 20 km west of Napoleon Bay, not found *in situ*, small diatreme dykes and sills (cemented with K-rich, peraluminous glass), 8 km WSW, and coeval, mineralogically similar lamproite dykes at Sisimiut, southwest Greenland.

**Keywords:** lamproite, ultrapotassic rocks, leucite, pseudoleucite, alkali amphibole, titanian mica, dyke reopening, peraluminous glass, Baffin Island, Northwest Territories.

### SOMMAIRE

Des filons verticaux post-tectoniques, d'orientation vers l'ouest ou le nord-ouest, d'âge protérozoïque, découverts à la baie de Napoléon, sur l'île de Baffin, aux Territoires du Nord-Ouest, contiennent des associations de minéraux typiques de lamproïtes: (1) phénocristaux de leucite ferrifère et de sanidine, phlogopite riche en Ti, olivine magnésienne et diopside, et (2) une pâte contenant phlogopite titanifère, sanidine riche en Fe et apatite. Sauf dans les cas de bordures figées, la leucite s'est déstabilisée en intercroissance de sanidine et de kalsilite, ou bien a été complètement remplacée par la sanidine. Les cristaux de phlogopite sont enrichis en Fe vers leur bordure, et deviennent donc de l'annite ou de la ferri-annite. La magnésio-arfvedsonite titanifère et potassique apparaît tardivement dans certains filons, et se trouve progressivement enrichie en Fe, pour devenir de l'arfvedsonite titanifère potassique. Dans quelques cas, aegyrine et augite aegyrinique (ici et là titanifère) forment une surcroissance sur le diopside. Plus rarement, et à un stade très tardif, possiblement encore magmatique, il y a développement de surcroissances de magnésio-arfvedsonite potassique sur l'amphibole riche en Fe, et de phlogopite et “ferriphlogopite” sur le mica riche en Fe. Sauf dans le cas de l'aegyrine et de l'augite aegyrinique, tous les silicates ferromagnésiens sont sous-saturés en  $\text{Si} + \text{IVAl}$ , le déficit moyen dans la position tétraédrique s'étendant de 15.7% dans l'annite et la ferri-annite (bordure des grains) jusqu'à 1.5% dans la magnésio-arfvedsonite (en surcroissance). Les lacunes apparentes dans la position tétraédrique pourraient être remplies par le  $\text{Fe}^{3+}$ . Parmi les minéraux des filons de Baffin qui sont caractéristiques des lamproïtes connues, il faut signaler les amphiboles sodiques-calciques riches en K et Ti, shcherbakovite, chromite riche en Ti, et un oxyde à K, Ti et Fe. Toutefois, certains minéraux mineurs n'avaient pas été signalés auparavant dans des roches lamproïtiques [pectolite, lorenzenite, barytolamprophyllite, calcioancylite-(Ce), djerfisherite], et l'enrichissement tardif en Na-Fe semble extrême pour une lamproïte. Il semble y avoir eu différenciation avec injections magmatiques répétées après la cristallisation première. Parmi les roches qui sont peut-être affiliées, il y a une roche volcanique porphyritique contenant l'association pseudoleucite (sanidine) – forstérite – diopside – phlogopite titanifère, retrouvée environ 20 km à l'ouest de la baie de Napoléon, mais non *in situ*, de petits filons et filons-couches de diatèmes cimentés par un verre potassique et hyperalumineux, 8 km à l'ouest-sud-ouest, et des filons contemporains de lamproïtes assez semblables dans leurs assemblages de minéraux, et découverts à Sisimiut, dans le sud-ouest du Groënland.

(Traduit par la Rédaction)

**Mots-clés:** lamproïte, roches ultrapotassiques, leucite, pseudoleucite, amphibole alcaline, mica titanifère, réouverture des filons, verre hyperalumineux, île de Baffin, Territoires du Nord-Ouest.

## INTRODUCTION

On Baffin Island, Northwest Territories (62°53'N, 65°21'W), metamorphic rocks of the Canadian Shield are intruded by narrow lamproite dykes. This adds an occurrence, in the Canadian northeast, to the belt of ultrapotassic rocks that extends from Wyoming to west Greenland, a distance of over 4000 km (Hogarth & Peterson 1996).

The initial discovery was made in 1992, during a search for unrelated metamafic and meta-ultramafic rocks of Martin Frobisher's mines, which were tested for gold four centuries ago (Hogarth *et al.* 1994). The Discovery Dyke was no ordinary dyke, nor an associate of local pre-orogenic basic or ultrabasic rocks, such as those of Frobisher's Countess of Sussex mine (Fig. 1). Preliminary tests showed the rock to be enriched in K and Ti, depleted in Si and Ca, and clearly post-tectonic.

The area was re-examined by the author in 1994 but, since 1992, the Discovery Dyke exposure (B; Fig. 2) had been covered by a tongue of frozen rubble. Further investigation revealed several small satellite dykes on both sides of the ice-filled valley, as well as six dykes in four areas nearby (A, C, D, E; Fig. 2). Additional exposures were found behind a reservoir of ice and debris, 2½ km northwest (F; Fig. 2). Detailed mineralogical study in Ottawa and Montreal followed.

This paper presents the mineralogical data. A paper on petrochemical characteristics is planned (Peterson & Hogarth, in prep.).

## GEOLOGICAL SETTING

The Proterozoic metamorphic rocks in southeastern Baffin Island were derived from igneous and sedimentary protoliths that have since been metamorphosed to the upper amphibolite or lower granulite facies (Blackadar 1967, Jackson & Morgan 1978). Biotite-orthopyroxene and biotite-hornblende gneisses predominate; biotite-almandine and biotite-sillimanite gneisses are comparatively rare. At Napoleon Bay (Fig. 2), weakly foliated, stark-white anorthosite is conformable with dark grey biotite-hornblende gneiss in three localities. Local "mafic gneiss" includes hornblende-plagioclase, diopside-plagioclase and diopside-orthopyroxene-plagioclase assemblages.

As a result of a traverse 100 km NNW, along strike with metamorphic strata at Napoleon Bay, Scott (1996) concluded that "the rocks... may represent the northward continuation of the ca. 1.9 Ga metaplutonic rocks of the Torngat orogen [northern Labrador]". This age is consistent with ages of high-grade metamorphism and plutonism in southeastern Baffin Island (Hogarth & Roddick 1989, Jackson *et al.* 1990, Hogarth *et al.* 1994). An episode at ca. 1.5 Ga marks the final metamorphism of the region, although this event may

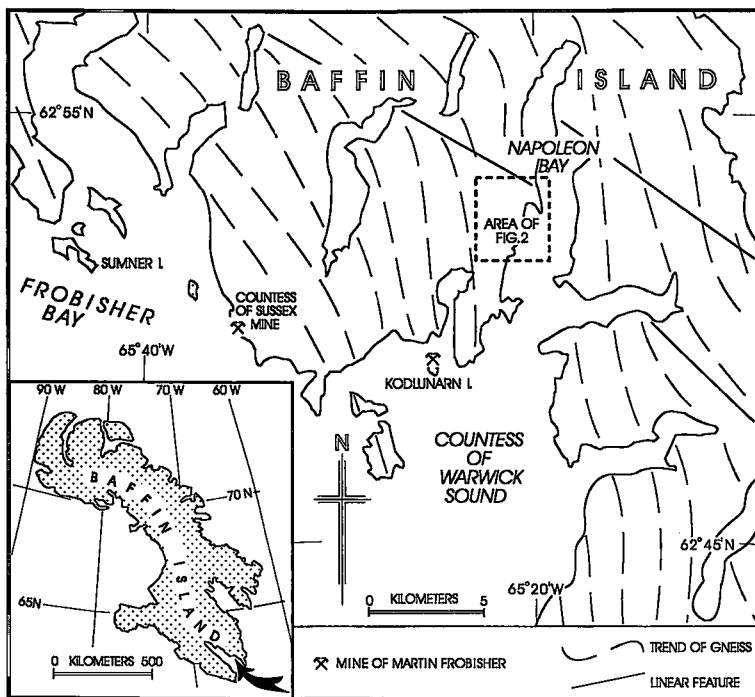


FIG. 1. Map locating sites mentioned in text.

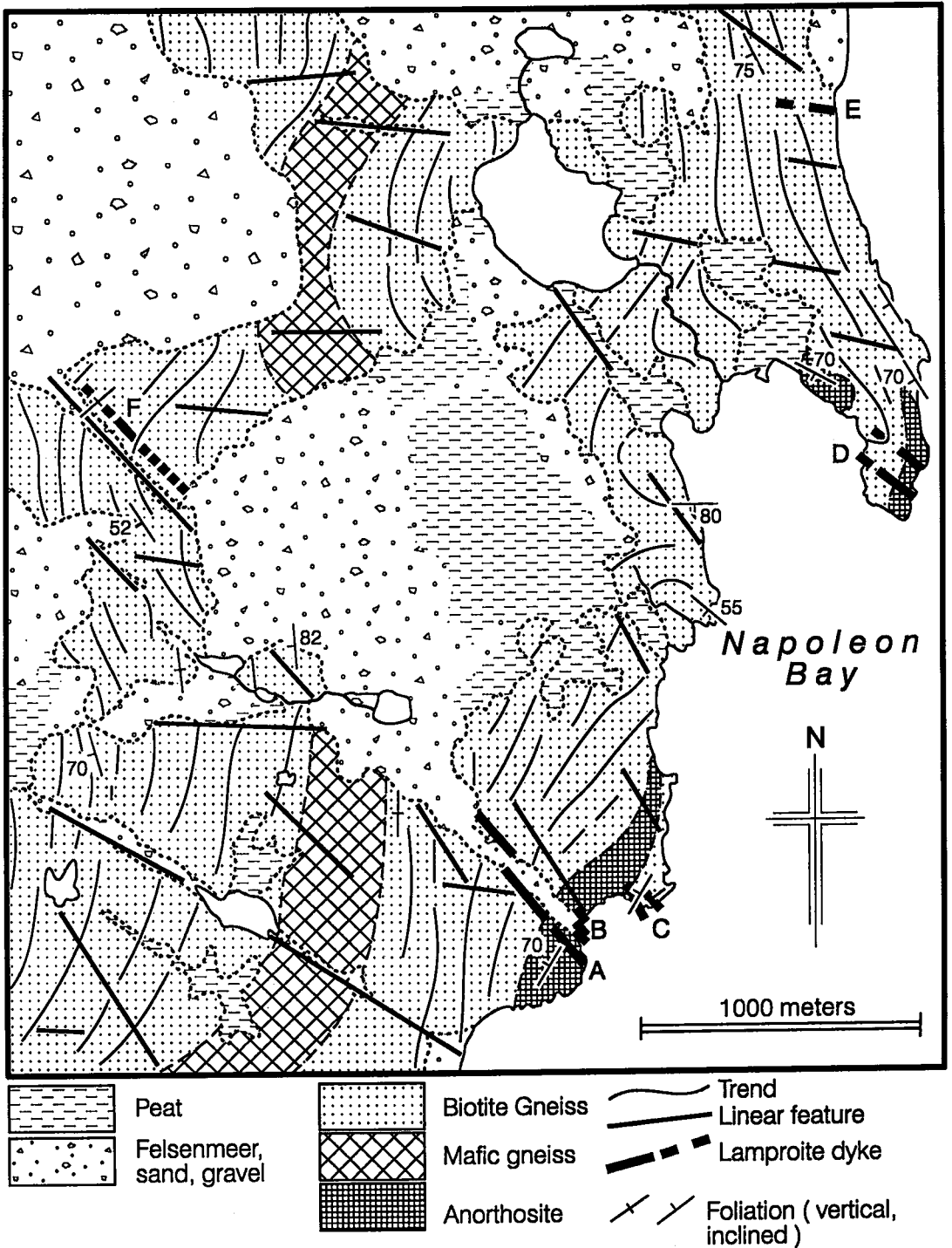


FIG. 2. Geology, ultrapotassic dyke area, Napoleon Bay, Baffin Island.

represent a "cooling age" [11 K–Ar determinations on metamafic and meta-ultramafic rocks reported by Hogarth *et al.* (1994)]. The pristine Baffin dykes, 1240 Ma old (T.D. Peterson; pers. comm.; K–Ar phlogopite age), appear to have penetrated a stabilized craton during post-orogenic relaxation.

At Napoleon Bay, the prevalent strike of the country-rock foliation is northerly (with numerous minor fluctuations), the dip, 50–80°W, and the plunge, 40–50°W. Pronounced joint patterns are NW- and W- to WNW-trending. The E–W set tends to converge landward (W), and the northwest set tends to converge seaward (SE).

#### FIELD RELATIONSHIPS OF POST-OROGENIC DYKES AND VOLCANIC ROCKS

Dark-colored, post-orogenic dykes are localized in both sets of linear features of southeastern Baffin Island. Those at locations A, B, C, D and F (Fig. 2) lie in northwest lineaments, but the dyke at E has an E–W trend. The dykes, henceforth called the Baffin dykes, are easily located by color contrast with the host rock, especially where the brownish black dykes intrude white anorthosite. They are also recessive, leaving vertical to sub-vertical clefts near the sea. Leucite and pseudoleucite are removed preferentially, commonly producing an indented, or even a perforated, surface.

The Baffin dykes are narrow and composite. The thickest (northern dyke of area D) is 2 m across and crops out, intermittently, along 270 m. Some dykes show internal (as well as marginal) chill-zones, easily identified in the field. For example, the 1.7-m-wide Discovery Dyke contains two internal chill-zones, and the 1.5-m-wide dyke at A contains seven internal chill-zones. A search for similar dykes nearby was unsuccessful, but possibly related occurrences at Sumner and Kodlunarn Islands (Fig. 1) deserve consideration.

A small black cobble was, in 1991, collected by Jamesie Sataa from the beach at Greater Sumner Island, about 20 km west of the study area. It is microcrystalline, with its rounded surface liberally perforated by tiny holes. Its pocked surface suggested a rock similar to the Baffin dykes, and provided an additional specimen for investigation.

In August 1983, two small intrusive bodies were located on the south side of Kodlunarn Island, 8 km SSW of the Baffin dykes, then called *hyaline dykes* (Hogarth & Gibbins 1984), but here termed *diatreme dykes* and *sills*, because they are largely composed of fragments, apparently derived from near-surface wall-rock by gaseous explosion. These occurrences were re-investigated in July 1992. One is a vein (partly concordant, partly discordant) cutting leucocratic biotite gneiss. It is up to 5 cm wide and can be followed along the seascarp for 4 m. The other is a narrow (1 cm wide) sill, traced for about 2 m.

#### METHODS OF RESEARCH

Polished thin sections for electron-microprobe analyses were made from the Baffin dykes, the beach cobble of Greater Sumner Island, the two diatremes on Kodlunarn Island, and country rocks. Minerals were analyzed with a JEOL 733 electron microprobe and wavelength-dispersion spectrometry (WDS); it is equipped with Tracor Northern 5500 and 5600 automation and housed in the Mineral Sciences Division of the Canadian Museum of Nature. Operating conditions were 15 kV, a beam current of 20 nA, and a beam 10–30  $\mu\text{m}$  in width. Data were collected for 25 s or 0.25% precision per element, whichever came first, and were reduced with a ZAF program. Calcite and some of the chromite grains were analyzed with the JEOL 8900L (WDS) electron microprobe at McGill University. Glass in the vitric diatreme sill on Kodlunarn was analyzed by Peter Jones at Carleton University, with a Cambridge Instruments MK4 electron microprobe (WDS).

Wherever possible, results of two, or preferably three or more, analyses from within a single polished thin section were averaged. The range within a cluster is shown, in parentheses, as standard deviation (Sx). Standard deviations of iron oxides are in terms of oxides reported in analyses (total iron expressed as  $\text{Fe}_2\text{O}_3$  in feldspars and feldspathoids, and as FeO in others). Weight per cent  $\text{Fe}_2\text{O}_3$ , FeO and  $\text{H}_2\text{O}$  were derived by calculation. Oxygen equivalents of F were subtracted in making totals. Oxides are based on 100% total (all constituents included) in tables using wt%, and in wt% values quoted in the text.

Nomenclature and formulae generally follow those of Nickel & Nichols (1991) and Nickel (1992). Abbreviations are those of Kretz (1983) or adapted from them. The following abbreviations are used in this paper

Cr†:	100 Cr/(Cr + Al)
Fe <sup>3†</sup> :	100 Fe <sup>3+</sup> /(Fe <sup>3+</sup> + Al)
Fe <sup>3*</sup> :	100 Fe <sup>3+</sup> /Fe
Fe†:	100 Fe/(Fe + Mg)
Mg†:	100 Mg/(Mg + Fe)
Mg*:	100 Mg/(Mg + Fe <sup>2+</sup> )
Ti†:	100 Ti/(Ti + Al + Cr)
$\Delta$ :	100 ( $Z_{\text{ideal}} - \text{Si} - \text{IVAl}$ )/ $Z_{\text{ideal}}$
Q:	dp – hd – fs – en quadrilateral
TE:	Sum of end members CaMg <sub>1/2</sub> Ti <sub>1/2</sub> AlSiO <sub>6</sub> and NaFe <sup>2+</sup> <sub>1/2</sub> Ti <sub>1/2</sub> Si <sub>2</sub> O <sub>6</sub>
$\Sigma_A$ :	Sum of A cations
$\Sigma_B$ :	Sum of B cations
$\Sigma_C$ :	Sum of C cations
$\Sigma_Z$ :	Sum of Z cations
apfu:	atoms per formula unit
n:	Number of electron-microprobe analyses processed within a compositional cluster

TABLE 1. MODAL COMPOSITION OF TYPICAL ROCKS

Section Area	T1 A	T2 B	T3 B	T4 B	T5 B	T6 D	T7 E	T8 F	T9 SI
felsic phases	38.7	17.1	14.6	41.4	49.0	34.2	30.2	25.9	13.5
"biotite"	34.0	g	g	26.8	22.5	39.0	25.3	21.9	1.3
brown am	0	0	0	0	1.5	2.7	15.5	0.6	tr
green am	0	0	0	0	tr	0.6	2.1	0.1	0
pink am	0.4	0	0	0.4	1.3	0.2	0.4	0.1	0
diopside	11.8	7.8	5.8	21.2	16.2	4.5	4.0	3.3	2.6
"green px"	3.5	g	g	2.9	1.4	3.5	0.2	g	tr
pectolite	1.6	0	0	0	0	0	0	0	0
"olivine"	5.4	3.6	3.2	3.2	0	10.8	2.4	2.8	8.2
titanite	1.6	0	0.2	1.8	0.1	0.8	0.2	0.1	tr
carbonates	1.4	0	0	0.7	g	2.2	15.7	7.4	g
apatite	0.6	g	g	0.6	0.1	tr	0.8	0.2	g
opaque phases	0.8	0	0.2	1.0	0.9	tr	0.9	2.4	g
others	0.2	0	0	0.1	tr	1.5	2.3	0.5	0
groundmass	0	71.5	75.9	0.0	6.9	0	0	34.7	74.4
points	7831	3177	3460	8790	8805	8308	9681	8157	6793
<i>Apparent average long dimension of phenocrysts (mm)</i>									
felsic phases	1.1	0.2	0.25	0.45	0.25	0.4	0.7	0.3	0.1
"olivine"	0.8	0.7	0.6	0.6	—	0.6	—	0.5	0.5
diopside	0.6	0.6	0.6	0.8	0.5	0.9	0.4	0.5	0.45
pectolite	0.4	—	—	—	—	—	—	—	—
brown am	—	—	—	—	0.1	0.5	0.8	<0.1	0.1
"biotite"	0.5	<0.05	<0.05	0.8	0.5	0.25	0.7	0.2	<0.05

*Thin sections:* T1, near marginal chill zone; T2, marginal chill zone, Discovery Dyke; T3, internal chill zone, Discovery Dyke; T4, coarse internal zone, Discovery Dyke; T5, center, 5-cm-wide satellite dyke; T6, near chill zone, 2-m-wide dyke; T7, near chill zone, 1-m-wide dyke; T8, center, 15-cm dyke; T9, beach cobble, Summer Island (SI). *Special abbreviations:* am, amphibole; g, included with groundmass; px, clinopyroxene. *Felsic phases* include leucite, kalsilite, sanidine; *olivine* includes olivine, chlorite, saponite, serpentine; *green pyroxene* includes aegirine and aegirine-augite; *biotite* includes all ferromagnesian micas; *others* include other minerals and unidentified species.

TABLE 2. MINERALS IN THE BAFFIN LAMPROITE SUITE

<i>A. Phenocrysts</i>	<i>D. Cavity Fillings</i>
sanidine	potassium magnesio-arfvedsonite
leucite	potassium arfvedsonite
phlogopite	calcite
"ferrilphlogopite"	magnetite
potassium magnesio-arfvedsonite	dolomite
potassium arfvedsonite	
diopside	<i>E. Groundmass and microminerals</i>
pectolite	zircon
olivine	titanite
	lorenzenite
<i>B. Replacement and retrograde products</i>	shcherbakovite
sanidine	phlogopite
kalsilite	barytolamprophyllite
aegirine	sanidine
aegirine-augite	galena
potassium ferro-richterite	sphalerite
potassium magnesio-katophorite	pyrite
magnesio-arfvedsonite	djerfisherite
potassium magnesio-arfvedsonite	TiO <sub>2</sub> (rutile?)
annite	ilmeneite
ferril-annite	magnetite
chlorite	ulvöspinel
saponite	chromite
chrysotile	perovskite
hematite	K-Ti oxide
calcite	calcite
dolomite	stromiämite
	dolomite
<i>C. Contact minerals</i>	calcio-anorthite (Ca)
diopside	barite
aegirine	fluorapatite
aegirine-augite	
lorenzenite	an unidentified Na-Zr silicate
muscovite	two unidentified Ca-Zr silicates
sanidine	an unidentified Mg-Ti silicate
"nepheline"	
magnetite	

### THE SUMNER ISLAND BEACH COBBLE AND KODLUNARN ISLAND DYKES AND SILLS

n.a.: Not analyzed  
n.c.: Not calculated  
N: Number of compositional clusters processed.

#### MINERAL ASSOCIATIONS

The mineral associations are summarized in Table 1. The mode is dominated by felsic phases, which includes pseudoleucite, leucite itself, and sanidine that does not replace leucite. Magnesium - iron micas, collectively termed "biotite", are somewhat less important. Less common are clinopyroxene (mainly diopside) and olivine. Together, these four groups, felsic phases, "biotite", clinopyroxene and olivine, commonly make up 95% of the rock volume, although amphibole and carbonate are important in parts of dykes at E and F. All of these minerals may be megacrystic, although "biotite" is late, and olivine is not present in the more evolved rocks.

Over 40 minerals occur in these rocks (Table 2), including small amounts of the rare species "[tetra] ferrilphlogopite", titanian potassium ferro-richterite, shcherbakovite, and a rare mineral similar to priderite.

The rock consists of phenocrysts and microphenocrysts in fine-grained groundmass. The largest phenocrysts (up to 2 mm in long dimension) consist of olivine, now mainly altered to a golden phyllosilicate. The phenocrysts are commonly seen in clusters, more rarely in rectilinear, cruciform twins (twin plane identified optically as the  $[h0l]$  zone). Similar olivine twins were described and illustrated by Gonnard (1909), in phenocrysts in volcanic rock (type not specified) from Cantal, France. At Sumner Island, microphenocrysts include diopside prisms, some rimmed with green aegirine-augite, some in stellate clusters, as well as equant crystals and clusters of crystals of sanidine, possibly remnants of pre-existing leucite. These phenocrysts and microphenocrysts show no preferred orientation. The groundmass is composed of diopside, biotite, titanite, perovskite (partly altered to titanite), chromite, barite, pyrite, calcite, and a carbonate close in composition to  $\text{CaSr}(\text{CO}_3)_2$ . Other, very fine-grained phases were beyond the range of microscopic and chemical identification.

The Kodlunarn dyke contains highly rounded to fractured fragments of wallrock. The extremely fine-

grained matrix included primary spicules of alkali feldspar ( $Or_{75.5}Ab_{23.8}An_{0.7}$ ), some radiating from quartz nuclei. A few slender prisms of ferro-actinolitic hornblende are interspersed. The matrix also contains magnetite, pyrite, apatite, indeterminate Fe–Al silicates, and tiny spherules of quartz, cored with ferroan dolomite and calcite.

The sill includes scattered patches of devitrified glass at the contact, which extend into the interior along fractures in unaltered glass. Numerous macro- and micro-scale rounded xenoliths (mainly feldspar and quartz) are cemented with yellowish brown glass, identified microscopically and analyzed by electron micro-

probe ( $n = 4$ ). This glass is rich in Al [17.8%  $Al_2O_3$ ,  $Al/(Ca + Na + K) = 1.6$ ], poor in Mg (4.3% MgO,  $Mg^\dagger = 50$ ), and rich in K [5.4%  $K_2O$ ,  $K/(Ca + Na) = 1.4$ ].

#### FELSIC PHASES IN THE BAFFIN DYKES

##### *Leucite, kalsilite, sanidine and "nepheline"*

Feldspars and feldspathoids are, collectively, the most abundant minerals of the Baffin dykes. Leucite, one of the earliest minerals, crystallizes as microphenocrysts in the chill zones, grows to a macroscopic size, but disappears in the coarse-grained fraction of the

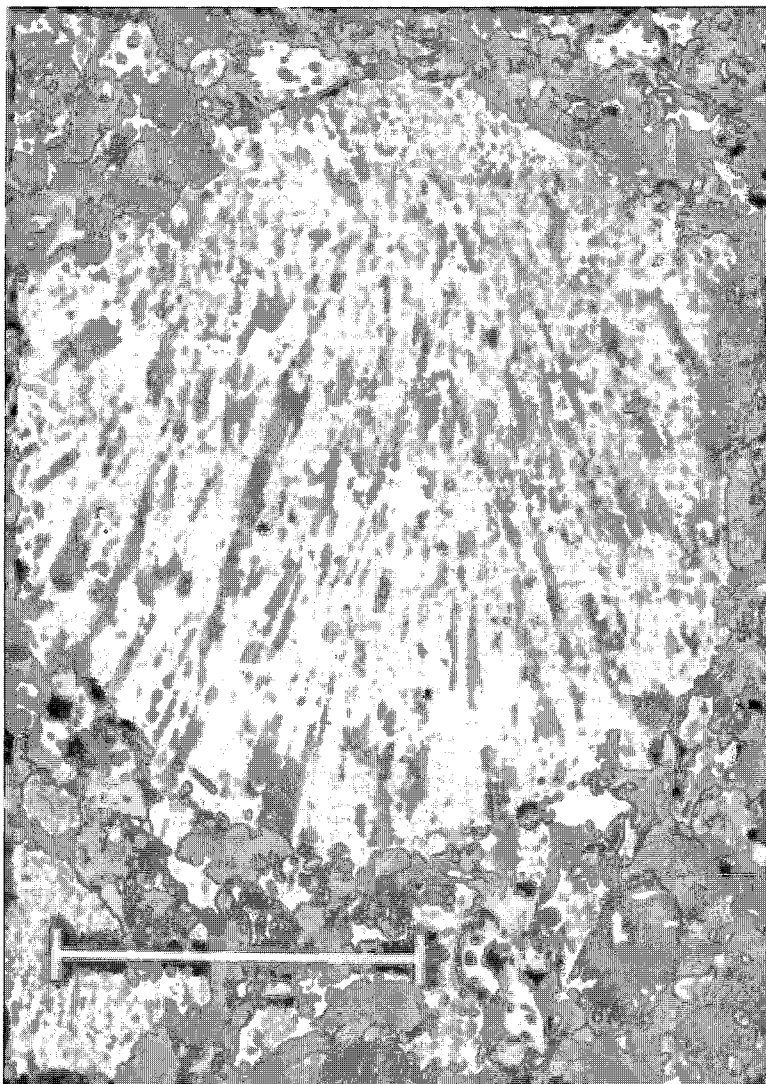


FIG. 3. Leucite crystal exsolved to kalsilite (light) and sanidine (dark). Surrounding minerals are phlogopite (variable shades of grey), sanidine (dark grey) and an unidentified Ti–Fe–K oxide (white). Back-scattered electron image. Area D. Bar scale 1.0 mm.

TABLE 3. SELECTED COMPOSITIONS OF FELSIC PHASES

No	alkali feldspar				kalsilite		leucite	"nepheline"
	S1	S2	S3	S4	K1	K2	L1	N1
n	1	2	1	6	2	3	3	9
Area	B		E		B	E	B	E
SiO <sub>2</sub>	64.76	63.22(90)	62.23	62.31(70)	37.70(32)	38.22(30)	55.48(88)	44.76(54)
Al <sub>2</sub> O <sub>3</sub>	18.26	19.00(62)	18.74	18.46(71)	31.14(54)	30.41(37)	22.39(44)	24.90(29)
Fe <sub>2</sub> O <sub>3</sub>	0.26	0.36(01)	0.06	0.70(42)	1.70(10)	1.52(23)	0.77(10)	0.18(02)
CaO	<0.02	0.03(01)	<0.02	<0.02	0.15(05)	<0.02	<0.02	9.45(17)
BaO	<0.03	<0.03	2.43	1.65(55)	<0.03	<0.03	<0.03	0.73(67)
Na <sub>2</sub> O	0.05	0.31(20)	0.16	0.12(03)	0.58(10)	0.54(20)	0.07(02)	13.97(19)
K <sub>2</sub> O	17.18	17.23(08)	15.58	16.12(63)	28.33(30)	28.66(36)	21.22(52)	5.68(21)
Total	100.51	100.15	99.20	99.36	99.60	99.35	99.93	99.67
Charge	16				64		12	64
Si	2.993	2.945	2.953	2.948	7.981	8.115	2.017	8.879
Al	0.995	1.043	1.048	1.029	7.769	7.609	0.959	5.821
Fe <sup>3+</sup>	0.009	0.013	0.002	0.025	0.271	0.243	0.021	0.027
Σ <sub>Z</sub>	3.997	4.000	4.004	4.002	16.021	15.967	2.998	14.727
Ca	0	0.001	0	0	0.034	0	0	2.008
Ba	0	0	0.045	0.031	0	0	0	0.057
Na	0.004	0.028	0.015	0.011	0.238	0.222	0.005	5.373
K	1.012	1.024	0.943	0.973	7.650	7.762	0.984	1.437
Σ <sub>A</sub>	1.017	1.053	1.003	1.015	7.922	7.984	0.989	8.875

Specimen numbers: S1 glass of sanidine composition, veinlet in anorthosite near dyke; S2 sanidine after leucite, phenocryst in marginal chill-zone; S3 sanidine coating joint surface in anorthosite, near satellite dyke; S4 sanidine after leucite, in marginal chill-zone; K1 kalsilite after leucite, coexists with S2; K2 kalsilite after leucite, in marginal chill-zone, coexists with S4; L1 leucite, internal chill-zone; N1 nepheline-like mineral, "islands" in glass, contact of dyke and hornblende gneiss. Proportion of major elements reported as oxides, in wt.%.

dykes, owing to overprint by sanidine as a decomposition product, replacement or as an independent mineral. Leucite (unaltered) is preserved in a single specimen from an internal chill-zone at the Discovery Dyke (the only internal chill-zone examined). It has the typical trapezohedral outline, twinning and optical properties of tetragonal leucite.

More commonly, pseudomorphs after leucite (Fig. 3) preserve the {211} outline, even in the largest crystals, and consist of tabular kalsilite, interleaved with sanidine. These packets (several units with distinct orientation per "crystal" of pseudoleucite) may represent domains of former tetragonal leucite and relics of transformation twins resulting from the cubic → tetragonal inversion.

Compositions of two pairs of coexisting sanidine and kalsilite S2 - K1 and S4 - K2 are listed in Table 3. These pairs appear to result through breakdown of tetragonal leucite according to the scheme:



This transition takes place sluggishly at ca. 500°C (atmospheric pressure; positive P-T slope), but P(H<sub>2</sub>O) enhances the breakdown (Scarfe *et al.* 1966, Gittins *et al.* 1980). Thus, in the Baffin dykes, leucite persists in the chill-zones, but underwent subsolidus decomposition in the more permeable, coarse-grained fractions. The intergrowth differs from that of sanidine-kalsilite in the alkaline Bathjerg intrusion, illustrated by Gittins *et al.* (1980; their Figs. 1A, B), but seems identical with

that of "pseudoleucite" in the Sisimiut lamproites, illustrated by Thy *et al.* (1987; their Fig 2c).

Feldspar has the optical properties of high sanidine (inclined dispersion,  $\nu > r$ ,  $2V_x \approx 45^\circ$ ,  $X \wedge (001) = 5^\circ$ ). Besides its formation during breakdown of leucite, sanidine occurs as discrete, unzoned phenocrysts that have had an independent origin (and from which the optical measurements were taken). Glass in the contact zone in the wallrock also has the composition of sanidine (Table 3, specimen S1), as material with isotropic optics and typical flow-structure. Sanidine is also present as microcrystals coating fractures in wallrock near the dykes (Table 3, specimen S3).

A narrow rind of cross-fiber "nepheline" separates dyke from wallrock in all six occurrences. The same mineral lines tiny fractures in wallrock near the dyke. These fibers had straight extinction and positive elongation, although some fibers in the wallrock have negative elongation. This mineral was extracted from a polished thin section and tested with X-ray powder diffractometry: its pattern is virtually indistinguishable from nepheline, but high levels of Ca and low levels of Al (Table 3, sample N1) suggest an unusual variant or new species. Further research on this material is in progress. "Nepheline", restricted to the exocontact of the Baffin dykes, has not been found with lamproites elsewhere.

Sanidine, leucite and kalsilite fit into restricted compositional domains that are close to end-member

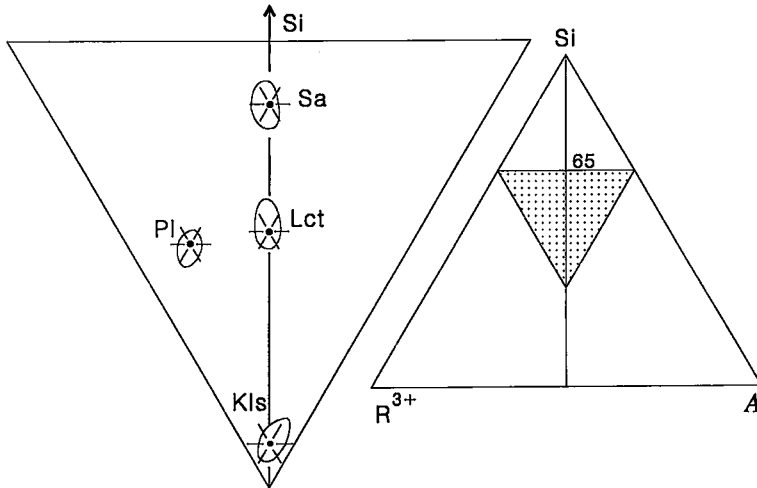


FIG. 4. Fields of sanidine (Sa;  $n = 15$ ), leucite (Lct;  $n = 3$ ), kalsilite (Kls;  $n = 4$ ) from Baffin dykes and volcanic rocks, and plagioclase (Pl;  $n = 3$ ) from wallrock, plotted on a Si –  $R^{3+}$  – A diagram. Individual plots have been omitted for simplicity. Ideal compositions are shown as six-rayed stars, with Pl representing  $An_{54}$ . A represents the alkalis.

compositions (Fig. 4). The relationship of kalsilite (Kls) and sanidine (Sa) to leucite (Lct) is clearly seen but, on this plot, the two varieties of sanidine overlap.

Compositions of coexisting kalsilite and sanidine, plotted on a  $Fe_2O_3$  –  $Na_2O$  diagram (Fig. 5), show that Fe and Na are selectively concentrated in kalsilite. The ten samples of primary sanidine plot in two fields: low-Fe (<0.3%  $Fe_2O_3$ ) and high-Fe (>1%  $Fe_2O_3$ ). The low-Fe field includes sanidine as joint coatings, glass of sanidine composition, and phenocrysts, considered to have formed independently of leucite decomposition. In contrast, there are four cases of high-Fe sanidine without associated kalsilite, including crystals from the Sumner Island cobble, which have vague trapezohedral outlines and are considered to have been derived from leucite. A high-Fe, low-Na glass, of sanidine composition, may genetically belong with the low-Fe group. Possibly, a high Na content rendered leucite unstable, with only low-sodium variants (like L1, Table 3) persisting through time.

Barium and Ca are distributed erratically in sanidine and kalsilite. Generally, Ba is concentrated in sanidine, Ca in kalsilite. Very minor Sr (ca. 0.1% SrO) is present in two crystals of sanidine, but was found to be below the detection limit (0.05%) in “nepheline”.

#### MICA AND AMPHIBOLE GROUPS

##### *Trioctahedral mica*

Phenocrysts of trioctahedral mica are abundant in all dykes, but are absent from the chill zones. The crystals have long dimensions of 0.2 to 0.8 mm and may account for 40% of the rock volume. In thin section,

they are red, brown, orange or yellow, and show various degrees of pleochroism. Like amphibole, pyroxene and some olivine, they are characterized by a shortage of Si + Al and, like most of the amphibole and some of the pyroxene, they have an unusually high content of Ti, as revealed by 30 compositions from seven dykes and the Sumner Island sample. Mica crystals are commonly zoned from a pale core to a dark margin. Some have a narrow overgrowth of pale mica. Less commonly, they are unzoned, such as the mica from Sumner Island and from a dyke at D.

In these samples of mica, the shortfall of Si + Al was balanced with  $Fe^{3+}$  in tetrahedral sites. The remaining iron was assigned to  $Fe^{2+}$  in octahedral sites, and the formula was calculated to an overall charge of 44.

In this study, mica species are classified according to their dominant ions as recommended by Nickel (1992), with end members *annite*:  $K_2Fe^{2+}_6Si_6Al_2O_{20}(OH)_4$ , *ferri-annite*:  $K_2Fe^{2+}_6Si_6Fe^{3+}_2O_{20}(OH)_4$ , *phlogopite*:  $K_2Mg_6Si_6Al_2O_{20}(OH)_4$  and “*ferriphlogopite*”:  $K_2Mg_6Si_6Fe^{3+}_2O_{20}(OH)_4$  (Nickel & Nichols 1991). Note that in this scheme, biotite intermediate between phlogopite and annite has no place. Accordingly, the mica compositions in the Baffin suite can be separated into four fields, divided at 50 Mg\* and 50  $Fe^{3+}$  (Fig. 6). The three core, margin and overgrowth triplets shown represent typical zonations: the early-formed core of crystals consists of phlogopite, the intermediate zones are annite – ferri-annite, and the outermost zones consist of phlogopite – “ferriphlogopite”. Unzoned mica at Sumner Island is rich in  $Fe^{2+}$ , but unzoned mica replacing forsterite at Napoleon Bay is poor in  $Fe^{2+}$ .

In the Baffin suite, titanium is the most distinctive element. Twenty-two compositional populations, after

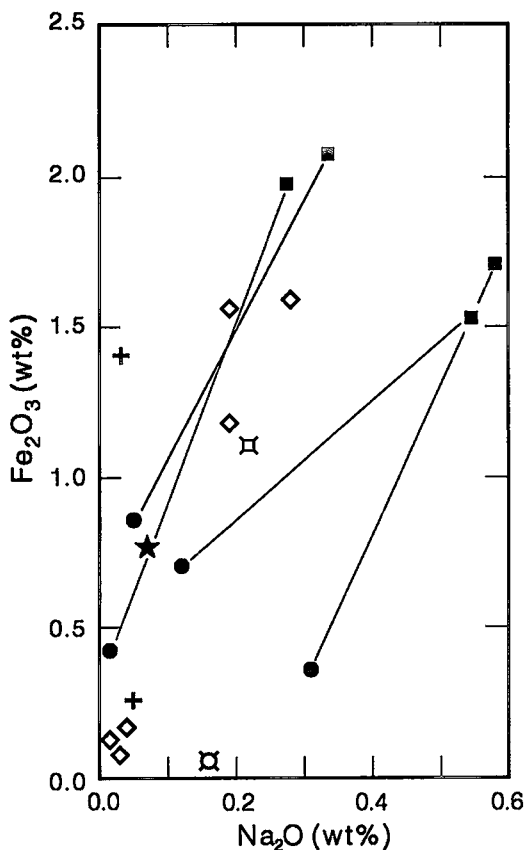


FIG. 5. Diagram showing  $\text{Fe}_2\text{O}_3$  and  $\text{Na}_2\text{O}$  in feldspar (sanidine, glass) and feldspathoids (kalsilite, leucite). Tie lines link sanidine with sanidine glass in the same polished thin section (four specimens, three dykes represented). Symbols: ■ kalsilite in Baffin dyke, ● sanidine associated with kalsilite, ◇ isolated sanidine crystals in Baffin dyke, □ sanidine crystals in wallrock near dyke, + glass of sanidine composition in wallrock near dyke, ▢ sanidine crystals in volcanic rock (Sumner Island cobble), ★ leucite in marginal chill-zone, Discovery Dyke.

normalizing totals to 100%, range from 5.38 (0.67 *apfu*) to 9.08 (1.06 *apfu*) and average 7.33 wt.%  $\text{TiO}_2$  (two anomalously low-Ti specimens with 2.98 and 3.25 wt.%  $\text{TiO}_2$  were excluded). Titanium tends to be highest in the core of crystals.

The  $\text{TiO}_2$  -  $\text{Al}_2\text{O}_3$  field outlined by Mitchell (1985; his Fig. 2) for phlogopite from lamproite of Western Australia and Montana accommodates seven of the Baffin core and margin pairs, one core (exterior unsuitable for analysis), and five cases of unzoned mica (Fig. 7). In addition, two pairs have compositions of grain margins that lie somewhat outside the field of mica compositions typical of lamproite. Although negative  $\text{TiO}_2$  slopes, core to margin, are relatively rare in mica from lamproite (Mitchell & Bergman 1991,

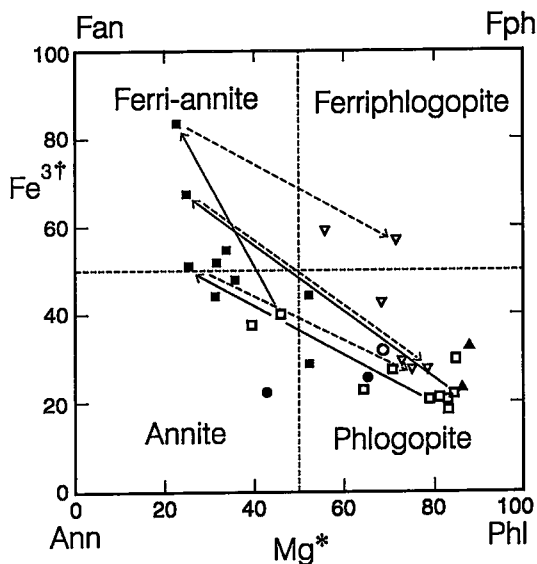


FIG. 6. Mica diagram, with end members ferri-annite, Fan ( $\text{KFe}_3^{2+}[\text{Si}_3\text{Fe}^{3+}\text{O}_{10}(\text{OH})_2$ ]; annite, Ann ( $\text{KFe}_3^{2+}[\text{Si}_3\text{Al}\text{O}_{10}(\text{OH})_2$ ]; phlogopite, Phl ( $\text{KMg}_3[\text{Si}_3\text{Al}\text{O}_{10}(\text{OH})_2$ ]; “ferriphlogopite”, Fph ( $\text{KMg}_3[\text{Si}_3\text{Fe}^{3+}\text{O}_{10}(\text{OH})_2$ ]). Arrows link core to margin to overgrowth (three triplets shown, three omitted for simplicity). Continuous-line arrows link compositions showing normal zonation, whereas broken-line arrows link compositions showing reverse zonation. Symbols: □ grain core, ■ grain margin, ▽ overgrowth, ▲ fosterite mantle, ○ unzoned crystal (dyke), ● unzoned crystal (volcanic).

p. 206), some mica pairs from lamproite at Sisimiut, Greenland (Scott 1981) and Hills Pond, Kansas (Mitchell 1985) have slopes similar to the Baffin suite. The four mica compositions reported by Cundari (1973) from central New South Wales cut across the upper part of the lamproite field; those from minette and Roman Province leucite plot to the left and above it (Mitchell & Bergman 1991, Fig. 6.33).

In Figure 8, compositions of the Baffin mica are compared, in terms of  $\text{Al}_2\text{O}_3$  and  $\text{FeO}^T$ , with mica from lamproite, worldwide. Cores of mica phenocrysts from Baffin dykes lie in the Al-rich end of the lamproite field, or on the Fe-rich side just beyond it. The exterior of these mica flakes departs further from the lamproite field, and extends into the Fe-rich, Al-poor area. This trend, although different from that of mica compositions in lamproite, shows similarities to the zonation of mica phenocrysts in orangeite from Sover North, South Africa (Mitchell 1995, Figs. 2.17, 2.24). However, the narrow overgrowths of light-colored, intermediate-Fe mica [“tetraferriphlogopite” absorption;  $\text{Fe}^T$  36.8 (9.0),  $N = 6$ ], in sharp contact with the exterior of the main crystal, a dark high-Fe mica [no differential absorption;  $\text{Fe}^T$  77.1 (4.6),  $N = 6$ ], seem to be peculiar to the Baffin dykes and differ from the zonation of low-Ti phlogopite

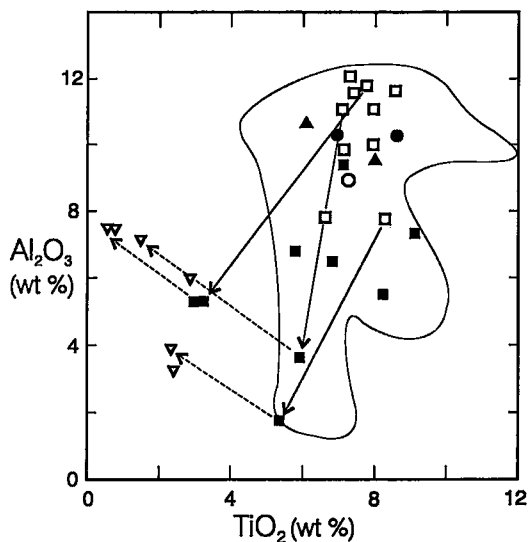


FIG. 7. The compositions of mica plotted in terms of  $\text{Al}_2\text{O}_3$  and  $\text{TiO}_2$ . Symbols are as in Figure 6, and arrows link the same compositions as in Figure 6. The plots fall mainly within the high-Ti, low-Al field outlined by Mitchell & Bergman (1991, Fig. 6.33), which is distinctive for mica from lamproite and certain ultrapotassic rocks in Uganda, but exclusive of mica for minette and volcanic rocks of the Roman Province (Mitchell & Bergman 1991, p. 214–215).

from carbonatites of Uganda (McCormick & Le Bas 1996), where Mg gradually increases toward the rim of the central crystal, which is overgrown by a low-Mg, low-Al mica, saturated with Si + Al at the very edge.

If A, Y, and Z represent interlayer, octahedrally and tetrahedrally coordinated ions in mica, respectively, the most important compositional variations in the suite can be explained by the following substitutional schemes (core to exterior of zoned grains) in decreasing order of importance:



Cation underfilling averages 10% in the Y position, 5% in the A position. Vacancies in A and a layer charge of approximately 1.0 are caused by the presence of divalent A cations and the substitution:

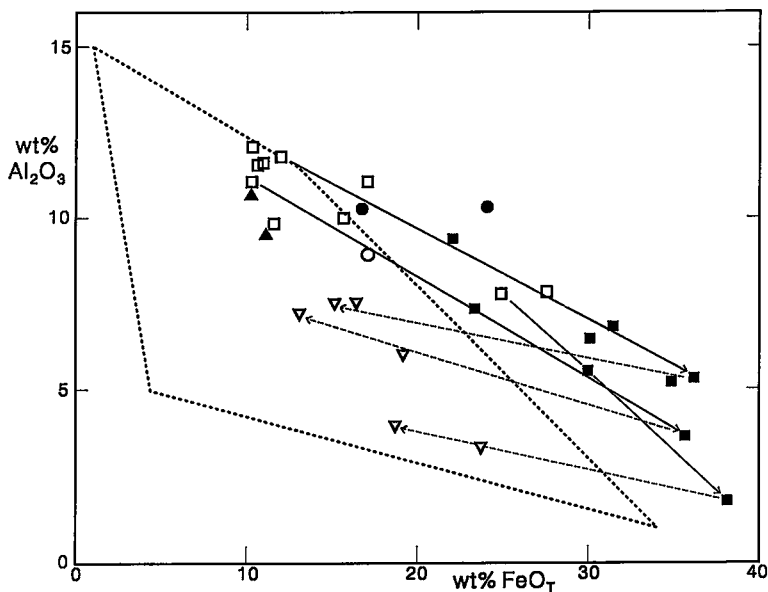


FIG. 8. Mica compositions plotted on an  $\text{Al}_2\text{O}_3$ – $\text{FeO}_T$  diagram. Symbols are as in Figure 6, and arrows link the same compositions as in Figure 6. The area outlined (data of Mitchell & Bergman 1991) circumscribes mica compositions in lamproitic rocks and excludes micas in the vast majority of igneous rocks.

TABLE 4. SELECTED COMPOSITIONS OF AMPHIBOLES AND MICAS

No. n Area	Amphiboles				micas				
	A1 3 B	A2 1 D	A3 6 E	A4 2 E	M1 3 A	M2 6 E	M3 9 E	M4 5 E	M5 5 nr.D
SiO <sub>2</sub>	48.20(13)	50.75	53.74(92)	44.64(08)	38.51(61)	37.03(24)	35.44(64)	40.88(52)	38.10(36)
TiO <sub>2</sub>	8.18(44)	2.20	5.85(26)	7.64(49)	6.14(43)	8.56(11)	6.86(53)	2.88(19)	1.13(22)
Al <sub>2</sub> O <sub>3</sub>	0.24(06)	0.21	0.04(01)	0.46(06)	10.83(60)	11.64(22)	6.49(57)	6.00(46)	18.58(19)
Cr <sub>2</sub> O <sub>3</sub>	<0.02	<0.02	0.23(06)	<0.02	<0.02	<0.02	<0.02	<0.02	<0.02
Fe <sub>2</sub> O <sub>3</sub>	4.22(19)	1.51	1.88(81)	8.76(74)	5.30(34)	4.83(42)	9.35(57)	6.88(54)	n.c.
FeO	21.37	21.51	11.76	21.22	5.54	6.62	21.75	13.01	9.65(47)
MnO	0.48(06)	0.69	0.07(02)	0.66(15)	0.07(01)	0.07(01)	0.30(07)	0.22(02)	<0.02
MgO	3.83(02)	7.60	11.96(65)	2.86(57)	19.57(97)	16.29(28)	6.78(32)	16.01(49)	18.83(55)
CaO	1.31(01)	4.37	0.33(12)	1.00(18)	0.04(02)	<0.02	<0.02	0.14(09)	0.14(04)
SrO	0.10(01)	n.a.	0.06(02)	0.16(00)	n.a.	0.05(02)	0.07(03)	<0.04	n.a.
BaO	<0.05	<0.05	<0.05	<0.05	1.11(17)	1.31(12)	0.46(12)	<0.05	0.23(04)
Na <sub>2</sub> O	6.29(02)	4.38	6.98(10)	6.17(07)	0.24(05)	0.22(01)	0.10(02)	0.32(10)	0.55(11)
K <sub>2</sub> O	4.45(07)	4.89	5.13(05)	4.43(03)	9.44(13)	9.35(08)	9.01(23)	9.81(32)	7.84(28)
F	0.19(08)	<0.1	0.39(14)	<0.1	0.64(05)	0.75(17)	<0.1	0.57(13)	0.34(07)
Cl	<0.02	<0.02	<0.02	<0.02	<0.02	<0.02	<0.02	<0.02	0.02(01)
H <sub>2</sub> O	<u>1.84</u>	<u>1.94</u>	<u>1.86</u>	<u>1.88</u>	<u>3.84</u>	<u>3.75</u>	<u>3.72</u>	<u>3.71</u>	<u>3.99</u>
Total	100.62	100.05	100.10	99.88	101.00	100.13	100.37	100.19	99.25
Charge	46				44				
Si	7.476	7.843	7.879	7.129	5.575	5.447	5.656	6.155	5.491
Al	0.044	0.037	0.007	0.086	1.848	2.018	1.221	1.065	2.509
Fe <sup>3+</sup>	0.480	0.120	0.114	0.785	0.578	0.535	1.123	0.780	0
Ti	0.954	0.256	0.645	0.918	0.668	0.947	0.824	0.326	0.122
Al	0	0	0	0	0	0	0	0	0.647
Cr	0	0	0.027	0	0	0	0	0	0
Fe <sup>3+</sup>	0.013	0.056	0.093	0.267	0	0	0	0	-----
Fe <sup>2+</sup>	2.772	2.780	1.442	2.835	0.670	0.814	2.903	1.638	1.163
Mn	0.062	0.090	0.009	0.090	0.009	0.009	0.041	0.028	0
Mg	<u>0.887</u>	<u>1.751</u>	<u>2.612</u>	<u>0.681</u>	<u>4.223</u>	<u>3.572</u>	<u>1.614</u>	<u>3.593</u>	<u>4.045</u>
Σ <sub>c</sub>	4.69	4.93	4.83	4.790	5.57	5.34	5.38	5.585	5.98
Ca	0.218	0.724	0.052	0.172	0.006	0	0	0.023	0.022
Sr	0.009	-----	0.005	0.015	-----	0.004	0.006	0	-----
Ba	0	0	0	0	0.063	0.076	0.029	0	0.013
Na	1.893	1.312	1.984	1.911	0.067	0.062	0.030	0.093	0.154
K	<u>0.880</u>	<u>0.964</u>	<u>0.959</u>	<u>0.903</u>	<u>1.743</u>	<u>1.755</u>	<u>1.834</u>	<u>1.884</u>	<u>1.441</u>
Σ <sub>d</sub>	3	3	3	3	1.880	1.897	1.900	2.00	1.63
F	0.093	0	0.181	0	0.293	0.347	0	0.271	0.155
Cl	0	0	0	0	0	0	0	0	0.005

Specimen numbers: A1 brown titanian *potassium arfvedsonite*, core of crystal; A2 pink titanian *potassium ferro-richterite*; A3 green *potassium magnesio-arfvedsonite*; A4 dark brown *potassium arfvedsonite*, exterior of crystal; M1 orange *phlogopite*, unzoned pseudomorph after forsterite; M2-M4 zoned phenocryst, M2 pale brown *phlogopite* core, M3 deep brown *amite* exterior, M4 pale brown *phlogopite* rim (overgrowth); M5 unzoned brown *phlogopite*, crystal from meta-ultramafic sill near D. The proportion of the major elements, except for F and Cl, is expressed as oxides, in wt.%.

Typical compositions are given in Table 4 and compared with a more normal *phlogopite* (higher Mg<sup>†</sup>, filled octahedral sites) from meta-ultramafic rock, a few tens of meters south of the dykes at D.

### Amphiboles

Amphiboles are minor, except in a sample from E, where in one specimen, their mode exceeds 17%. Brown is the most common color in transmitted light, green is local, and pink is rare. The habit is prismatic, with some prisms fanning out from a silicate interface into calcite segregations. Very fine-grained pink amphibole seems to replace pyroxene and olivine; rare blue amphibole overgrows brown at one locality. At area E, amphiboles are most common near internal chill-zones.

The chemical formula of amphiboles from the Baffin dykes is characterized by a high sum of K, Na and Ca

ions [Σ in the range 3.01 – 3.11;  $\bar{x}$  = 3.05 (03); 15 populations, 4 specimens], if calculations are based on 46 charges. Similar calculations produce high totals for most examples of amphibole from other lamproites. For example, six of the nine compositions in Mitchell & Bergman (1991, Table 6.22) from the Mt. Bayliss (Antarctica) lamproite also yield high A + B sums if calculated according to charge [Σ in the range 3.04 – 3.19;  $\bar{x}$  = 3.12 (05)]. Assuming that the analytical data on the Baffin amphiboles correct, the offending formulae can be explained as follows: the cations have a total charge in excess of 46, resulting in oxygen at O(3) rather than F and OH, or K + Na + Ca should be calculated to 3 ions (or less), resulting in a cation deficiency in octahedral sites. In this paper, the latter model is chosen, with K + Na + Ca = 3, thus permitting resolution of Fe<sup>2+</sup> and Fe<sup>3+</sup>.

The assignment of ions to tetrahedral sites imposes an additional problem. When dealing with potassium

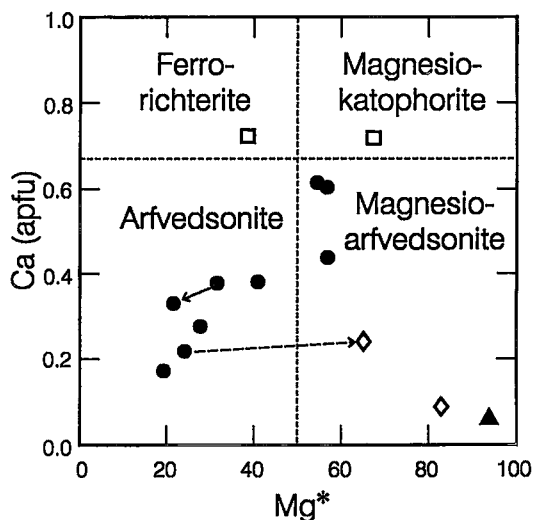


FIG. 9. Amphiboles from Baffin dykes plotted with respect to Ca and Mg\*. Two types of zonation are shown: normal or transitional, core to margin (short arrow), and reverse or abrupt, margin to overgrowth (broken-line arrow). Two trends are shown for simplicity. Symbols: □ pink sodic-calcic amphibole, ● brown alkali amphibole, ◇ green alkali amphibole, ▲ blue alkali amphibole.

richterite undersaturated in Si + Al, Oberti *et al.* (1992) filled vacant tetrahedral sites with  $Ti^{4+}$  in preference to  $Fe^{3+}$ . However, the amphiboles considered by these authors contained comparatively little Fe, and in the Baffin suite, T ions have been provisionally assigned in the order Si, Al,  $Fe^{3+}$ . Ti was accommodated in the octahedral sites, thus facilitating a  ${}^{VI}Fe^{2+} \rightarrow {}^{VI}Ti^{4+}$  charge transfer in the strip of octahedra and contribut-

ing to a marked pleochroism and absorption, *e.g.*, for amphibole A4, Table 4, *a* is rich yellow brown, *b* opaque and *c* chocolate brown;  $b \gg c > a$ .

Amphiboles range from sodic-calcic (pink) to alkali (brown, blue, green). Sodic-calcic amphiboles have  $0.67 < Ca < 1.34$  apfu, and Mg-rich and Mg-poor members have Si greater and less, respectively, than 7.5. Conversely, the alkali amphiboles of the Baffin suite have  $Ca < 0.67$  apfu, and  $Fe^{3+} > {}^{VI}Al$ . On a Ca-Mg\* diagram, these features permit, according to Leake (1978), a four-fold division of the 15 amphibole compositions into the fields of *ferrichterite*, *magnesio-katophorite*, *magnesio-arfvedsonite* and *arfvedsonite*, as shown on Figure 9. One composition of pink amphibole and nine of brown amphibole lie on a trend extending from magnesio-katophorite, through magnesio-arfvedsonite, to arfvedsonite, with Fe-rich brown amphibole later than Mg-rich, as shown by a zoned crystal from area C (solid arrow, Fig. 9). This trend is similar to the richterite  $\rightarrow$  arfvedsonite trend of Thy *et al.* (1987). Some overgrowths reverse this trend (*e.g.*, overgrowth at B, broken-line arrow, Fig. 9).

*Titanium* is higher here than in most examples of igneous amphiboles, worldwide. Except for a secondary blue amphibole at C (with 0.3%  $TiO_2$ ), the amphiboles of this study contain 2.2 (pink) to 8.1 (brown), and average 5.5 wt%  $TiO_2$ . These very high Ti (but low Al) contents are similar to amphibole from lamproites (Mitchell & Bergman 1991, Fig. 6.41). Eleven of the 15 amphibole compositions (Fig. 10) traverse the amphibole field of lamproite and lie outside the fields of leucitite, MARID-suite xenoliths, minette and kajanite, a diopside - leucite - nepheline - phlogopite - olivine volcanic rock (Mitchell & Bergman 1991, p. 90, 232).

The level of potassium is also high; it ranges from 4.3 (brown) to 5.2%  $K_2O$  (green) and, by itself, fills the

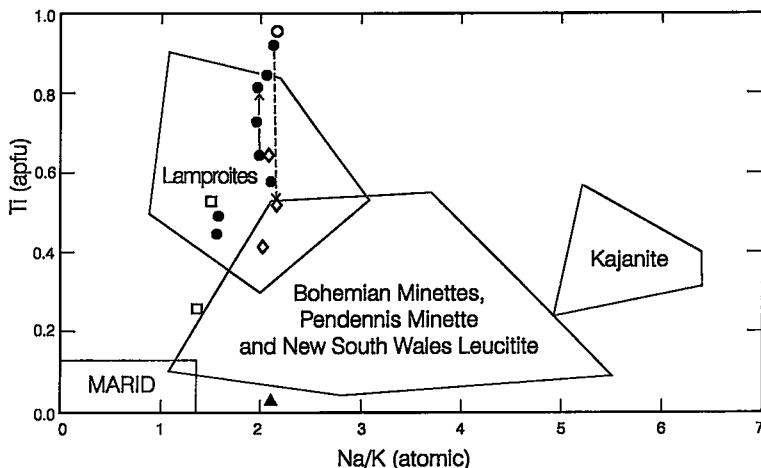


FIG. 10. Variation of Ti with respect to Na/K in amphiboles. Compositional fields have been adapted from Mitchell & Bergman (1991, Fig. 6.41). Symbols are as in Figure 9, and arrows link the same compositions as in Figure 9.

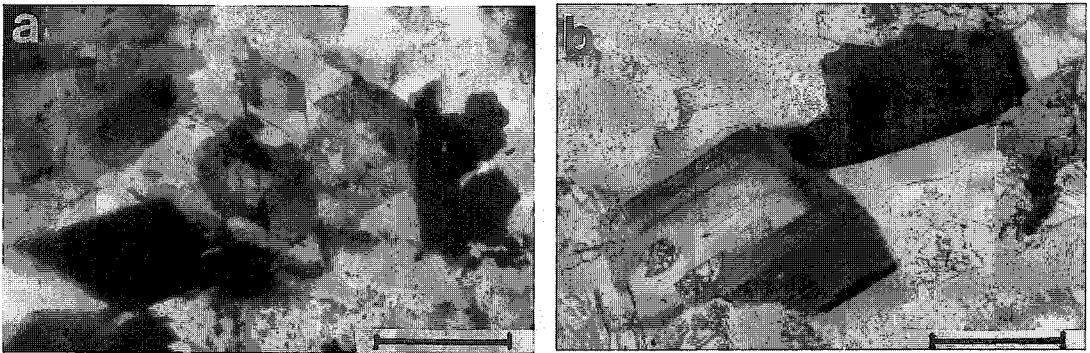
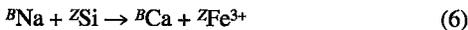


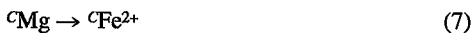
FIG. 11. a. Amphibole cross-sections showing extinction of {010} in Mg-rich overgrowths. b. Crystals of phlogopite (core) transitional to annite (margin), with an overgrowth of very pale phlogopite. Area E; photomicrograph; plane-polarized light. Bar scale = 0.2 mm.

A site almost completely. The decrease in Na/K from the normal level of 2 to 1.5 (Fig. 10) in a dyke at D, is due, not to an increase in K, but to the substitution of Na by Ca according to the scheme



All amphibole compositions have low Si + Al, which fills 93 (brown) to 99% (blue) of the available tetrahedral sites. Low-Mg amphiboles have the lowest Si + Al filling, high-Mg amphiboles have the highest. Thus late brown arfvedsonite has lower Si + Al than early brown magnesio-arfvedsonite, but late, mantling, blue and green amphiboles do not follow this paragenesis.

Octahedral sites are incompletely filled, with 89 to 99% of the available positions occupied. Amphibole compositions having low Si + Al, low C-ion totals, high Ti and high K were all described from lamproites by Mitchell & Bergman (1991, p. 218–232). In the brown amphiboles from the Baffin suite, the major compositional variations can be explained by the following substitutional schemes



Compositions of four amphiboles that characterize the extreme range of composition are given in Table 4. The Baffin suite of amphibole compositions resemble, in many respects, those from known lamproites. However, the variable, but generally low, magnesium numbers ( $\text{Mg}^\dagger$  14–75, average 42;  $n = 15$ ,  $N = 4$ ), and high Na contents, are not typical of lamproites.

#### Zoned amphiboles and micas in specimen 5101A (area E)

Strongly zoned phenocrysts of amphibole, with a sharply defined rim (overgrowth), were analyzed from three dykes (three compositional clusters), and zoned crystals of mica, also with a sharply defined rim, were analyzed from four dykes (six compositional clusters). The general trend, for both, is a continuous transition in color, from a light tan core to a deep brown exterior, which in some cases is overgrown by a narrow rim, pale green in amphibole, pale orange in mica.

Typical are strongly zoned amphibole and mica grains in specimen 5101A (Figs. 11a, b), taken from the dyke at E. The overgrowth preferentially extends *c* of the host mica and *b* of the amphiboles, ultimately changing the crystal habit of the latter by disappearance of {010}, with {110} only present in the prism zone but, in a few amphibole crystals, the overgrowths extend the prism length. Especially pronounced is the optical absorption of micas. Differential absorption notably decreases on traversing a phenocryst from pale core ( $AX \ll AZ'$ ) to an almost opaque exterior, where biabsorption and pleochroism are not evident (*i.e.*,  $AX \approx AZ'$ ). These margins, therefore, differ in absorption from the high-Fe, low-Al mica described by Veres *et al.* (1955), Wones (1963), Rimsakaya-Korsakova & Sokolova (1964) and Miyano & Miyano (1982), where  $AX > AZ'$ . The reason for this discrepancy is unclear; it may be connected with unusually high Ti in mica of the Baffin suite, which is lacking in mica studied by the above-cited authors, and is the only significant difference in composition. The dark mica reverts to pale mica on the extreme rim, here unzoned and with a reversed absorption-scheme, *i.e.*,  $AX > AZ'$  ("reversed pleochroism"). The Al + Si deficit in the *T* site is about the same as mica in the core, which has a normal absorption-scheme, *i.e.*,  $AZ' > AX$  ("normal pleochroism"). However, Ti is much lower (1/3 of the ions in the core; 1/3 to 1/13 in the other specimens). Octahedrally coordinated

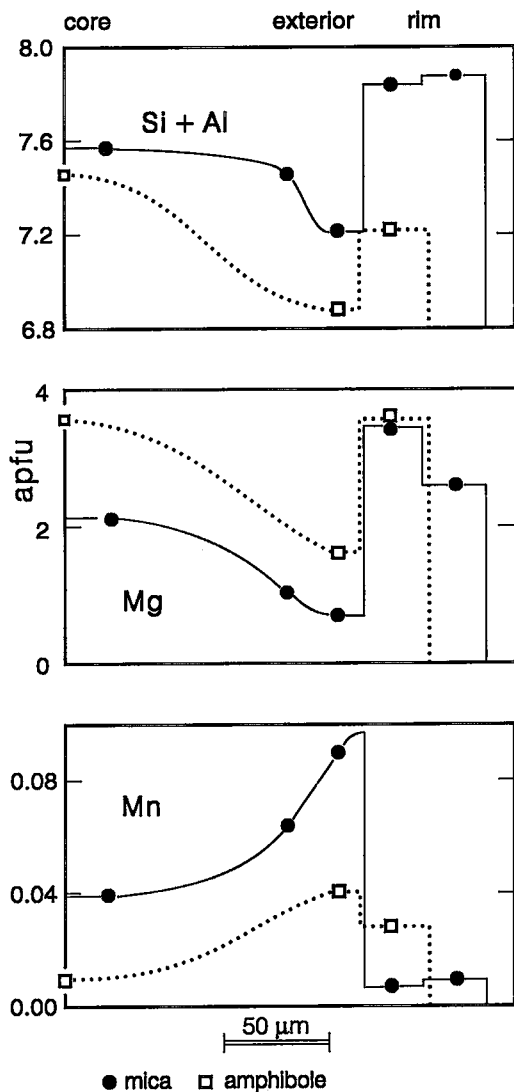


FIG. 12. Zoning in micas and amphiboles of area E.

Ti may strongly enhance in-plane charge transfer, in agreement with the findings of Rossman (1984).

Figure 12 is based on results of WDS electron-microprobe analyses and energy-dispersion spectra (EDS) and image observations of specimen 5101A. It shows patterns characteristic of all zoned grains of amphibole and mica in the dykes: progressive compositional variation from core to exterior paralleling the color transitions with, in some crystals, a marked change on the extreme rim. Table 5 summarizes chemical trends. In a few grains of amphibole, an area of low density of back-scattered electrons (BSE) is evident within the rim, corresponding to low Fe concentration.

TABLE 5. ZONATION TRENDS IN AMPHIBOLES AND MICAS IN DYKE AT 'E'

	Amphiboles		Micas	
	Core to exterior	Rim	Core to exterior	Rim
Si + Al	decreases progressively	increases	decreases progressively	increases
Ti	increases slightly	decreases	normally decreases	decreases further
Cr	always bdl	sadl	always bdl	sadl; some bdl
Fe	increases progressively	decreases	increases progressively	decreases
Mn	increases progressively	decreases	increases progressively	decreases
Mg	decreases progressively	increases	decreases progressively	increases
Ca	decreases progressively	decreases further	behaves inconsistently	
Sr	low throughout	decreases further	low throughout	decreases further
Ba	always bdl	bdl	decreases progressively	bdl
Na	increases progressively	increases further	increases progressively	increases further
F	decreases progressively	increases	decreases progressively	increases

Abbreviations: bdl below detection limit, sadl slightly above detection limit. Minimum detection limits: 0.02% Cr<sub>2</sub>O<sub>3</sub>, 0.04% SrO, 0.05% BaO, 0.1% F.

Amphiboles and micas exhibit similar patterns of zonation. The close similarity in grains of amphibole and mica cannot be fortuitous. The few differences are minor, and are either inconsistent (Ti and Ca) or structurally controlled (Ba). Both of these mineral groups formed late in the crystallization history; it is possible that the overgrowths were contemporaneous and formed as result of dyke reopening and introduction of magmatic fluid.

#### PYROXENE, PYROXENOID AND OLIVINE GROUPS

##### *Clinopyroxenes and pectolite*

The major pyroxene is long-prismatic diopside, colorless in thin section, with some crystals twinned on {100}. A few prisms are rimmed by grass-green aegirine-augite (more rarely, deep green to brownish green aegirine); in the matrix, some isolated tiny grains of aegirine-augite and aegirine are independent of diopside. At locality C, rare pale blue-green diopside overgrows prisms of brown amphibole and develops as acicular crystals within fans of amphibole; at B, deep green aegirine-augite mantles brown amphibole and replaces colorless diopside.

Paragenetic relationships, such as veining and zoning, indicate two main types of pyroxene, viz., early colorless diopside and late green aegirine-augite, which replaces diopside as diffuse patches and tips to prisms. Early diopside is oscillatory zoned, with a tendency to be more Na- and Fe-rich at the rim than at the core (e.g., C4 and C5, Table 6). These early crystals develop from Di<sub>95</sub>Hd<sub>4</sub>Ae<sub>1</sub> along the diopside - hedenbergite trend, reaching a final composition of about Di<sub>72</sub>Hd<sub>20</sub>Ae<sub>8</sub> (Fig. 13a). Beyond this point, the trend shifts toward aegirine [Ca + (Mg, Fe<sup>2+</sup>) → Na + Fe<sup>3+</sup>], with enrichment in Ti, according to the scheme Mg + 2Si → Ti + 2(Al, Fe<sup>3+</sup>) [substitution 4 of Morimoto (1989)]. Titanium-rich pyroxene can be considered in terms of the hypothetical end-members Ca Mg<sub>1/2</sub>Ti<sub>1/2</sub>AlSiO<sub>6</sub> and Na Fe<sup>2+</sup><sub>1/2</sub>Ti<sub>1/2</sub>Si<sub>2</sub>O<sub>6</sub>, with a maximum of 16 mol.% Ti end-members (TE), in a TE-Di-Ae system (Fig. 13b), or 13 mol.% when all end members are considered,

TABLE 6. SELECTED COMPOSITIONS OF PYROXENES, PECTOLITE AND FORSTERITE

No. Area n	Pyroxenes						Pectolite	Olivine		
	C1	C2	C3	C4	C5	C6	D1	F1	F2	F3
	A			B			A	A		S
	4	3	2	6	2	4	5	2	2	17
SiO <sub>2</sub>	52.84(17)	51.28(16)	51.32(07)	52.39(58)	50.78(42)	51.30(55)	53.81(36)	40.00(16)	38.40(30)	36.16(28)
TiO <sub>2</sub>	1.15(09)	2.80(50)	<0.02	1.28(16)	1.84(11)	8.57(56)	<0.02	<0.02	<0.02	<0.02
Al <sub>2</sub> O <sub>3</sub>	0.67(03)	0.34(08)	0.12(06)	0.84(26)	1.16(01)	0.21(10)	0.03(01)	<0.02	<0.02	<0.02
Cr <sub>2</sub> O <sub>3</sub>	0.48(09)	0.03(02)	<0.02	0.39(22)	0.12(05)	<0.02	<0.02	<0.02	<0.02	<0.02
Fe <sub>2</sub> O <sub>3</sub>	1.91	19.30	33.30	2.40	4.19	10.73	0.44	1.77	0.98	0.00
FeO	1.66(15)	6.33(13)	0.00(14)	1.72(24)	2.84(34)	10.94(98)	0.05(09)	9.43(27)	18.30(21)	34.77(54)
MnO	0.08(02)	0.36(09)	<0.02	0.08(01)	0.10(02)	0.25(06)	0.36(10)	0.15(01)	0.40(01)	0.50(03)
MgO	17.12(06)	2.11(10)	0.08(04)	16.67(21)	14.68(35)	1.88(89)	0.16(05)	48.54(16)	41.18(16)	28.64(49)
CaO	23.92(16)	7.25(34)	0.16(06)	24.08(21)	22.98(59)	5.43(99)	32.49(31)	0.28(01)	0.16(14)	<0.02
SrO	n.a.	n.a.	n.a.	n.a.	n.a.	0.07(03)	n.a.	n.a.	n.a.	n.a.
Na <sub>2</sub> O	0.28(02)	9.51(15)	13.20(03)	0.31(06)	0.80(16)	10.25(49)	9.38(05)	<0.03	<0.03	<0.03
K <sub>2</sub> O	<0.02	<0.02	<0.02	<0.02	0.05(04)	0.02(01)	<0.02	<0.02	<0.02	<0.02
H <sub>2</sub> O	0.00	0.00	0.00	0.00	0.00	0.00	2.69	0.00	0.00	0.00
Total	100.13	99.31	98.18	100.16	99.54	99.66	99.41	100.17	99.42	100.07
Cations	4						6	3		
Charge	12						17	8		
Si	1.931	1.986	2.005	1.919	1.892	1.974	2.996	0.984	0.990	1.001
Al	0.029	0.014	0	0.036	0.051	0.010	0.002	0	0	0
Fe <sup>3+</sup>	0.040	0	0	0.045	0.057	0.017	0.002	0.016	0.010	0
Ti	0.032	0.082	0	0.035	0.052	0.248	0	0	0	0
Al	0.000	0.002	0.006	0.000	0.000	0.000	0.000	0	0	0
Cr	0.014	0.001	0	0.010	0.003	0	0	0	0	0
Fe <sup>2+</sup>	0.013	0.562	0.979	0.021	0.061	0.294	0.017	0.017	0.009	0.000
Fe <sup>3+</sup>	0.051	0.205	0	0.053	0.088	0.353	0.002	0.194	0.395	0.805
Mn	0.002	0.012	0	0.002	0.003	0.008	0.017	0.003	0.009	0.012
Mg	0.932	0.121	0.005	0.910	0.815	0.108	0.013	1.799	1.583	1.182
Ca	0.936	0.301	0.00	0.945	0.917	0.224	1.938	0.007	0.004	0
Sr						0.002				
Na	0.020	0.714	1.000	0.022	0.057	0.765	1.013	0	0	0
K	0	0	0	0	0.002	0.001	0	0	0	0
OH	0	0	0	0	0	0	1	0	0	0
Mg <sup>†</sup>	90.0	13.7	0.5	88.5	79.8	14.0	39	88.7	79.3	59.5
Mg <sup>*</sup>	94.8	37.3	100	94.5	90.2	23.4	85	90.2	80.0	59.5
Si + Al	1.960	2.002	2.010	1.955	1.943	1.983	2.998	0.984	0.990	1.001
Q	98.0	30.5	0.6	97.7	94.1	50.8				

Specimen numbers: C1 colorless *diopside*, near edge dyke; C2 green *aegirine - augite*, replaced tip of C1; C3 brownish green *aegirine*, isolated grain, near edge dyke; C4, C5 zoned grain, core and rim, respectively, of colorless *diopside*, main dyke; C6 blue *titanian aegirine-augite*, satellite dyke; D1 *pectolite*, near edge dyke; F1, F2 colorless, zoned *olivine*, core and rim, respectively, near edge dyke; F3 unzoned *olivine*, meta-ultramafic sill, 15 km west-southwest of dykes (area S). The proportion of the major elements is expressed as oxides, in wt.%.

equivalent to 2.3 wt% TiO<sub>2</sub>. A small but persistent Cr content (normally 0.4 – 0.8 wt% Cr<sub>2</sub>O<sub>3</sub>) and low Mn (ca. 0.1% MnO) characterize this early pyroxene.

No "main-line" pyroxene compositions were observed between Ae<sub>8</sub> and Ae<sub>37</sub> (Fig. 13a), at which point green *aegirine-augite* appeared. One *diopside* phenocryst (area A), with a composition Ae<sub>1</sub>, was mantled by *aegirine-augite*, Ae<sub>70</sub> (Fig. 13a; C1 and C2, Table 6). *Aegirine-augite* developed along the *diopside-aegirine* trend line as the concentration of Ti decreased from ca. TE<sub>20</sub> (TE–Di–Ae system; Fig. 13b) to TE<sub>0</sub>, mainly according to the scheme Fe<sup>2+</sup> + Ti → 2Fe<sup>3+</sup>. The *aegirine-augite* contains appreciable Mn (0.2 – 0.4% MnO) but little Cr (<0.1% Cr<sub>2</sub>O<sub>3</sub>). However, the final *aegirine* (pyroxene C3, Table 6) contains no detectable Ti, Mn or Cr. The concentration of strontium in pyroxenes (all types) is invariably low (ca. 0.1% SrO).

Some compositions of blue-green to blue pyroxene of areas B and C do not follow the trend of "main-line" pyroxenes: they are particularly rich in Ti (4.6 – 8.6 wt% TiO<sub>2</sub>; e.g., pyroxene C6, Table 6). Depth of color appears to depend on Ti content, with the most Ti-rich crystals giving the deepest blue (navy blue with

E || b). Plots lie mainly below the *diopside-aegirine* trend line on the Di–Hd–Ae diagram (Fig. 13a) and above the *diopside - aegirine* trend on the TE–Di–Ae diagram (Fig. 13b). Grains contain appreciable Mn (0.3 – 0.6% MnO), but no detectable Cr. These variants, found in matrix and as overgrowths on phenocrysts, are relatively late in the paragenetic sequence; in one instance, Ti-rich *aegirine-augite* mantles potassium *arfvedsonite*.

Such Ti-rich pyroxene compositions are not restricted to the Baffin suite. For example, clinopyroxene grains containing up to 8% TiO<sub>2</sub> were described from malignite, syenite and metasomatized gneiss of the Red Wine alkaline complex, in central Labrador, by Curtis & Gittins (1979). Here depth of color (blue) also depends on the amount of Ti present, and was ascribed to a strong absorption peak centered at 665 nm (Abu-Eid 1976). Strens *et al.* (1982) assigned it to a Fe<sup>2+</sup> → Ti<sup>4+</sup> charge transfer. The blue-green to blue color of pyroxene grains in the Baffin suite may be due to the same mechanism.

Tetrahedral sites, in colorless and blue-green crystals, appear to be slightly undersaturated in Si + Al (e.g.,

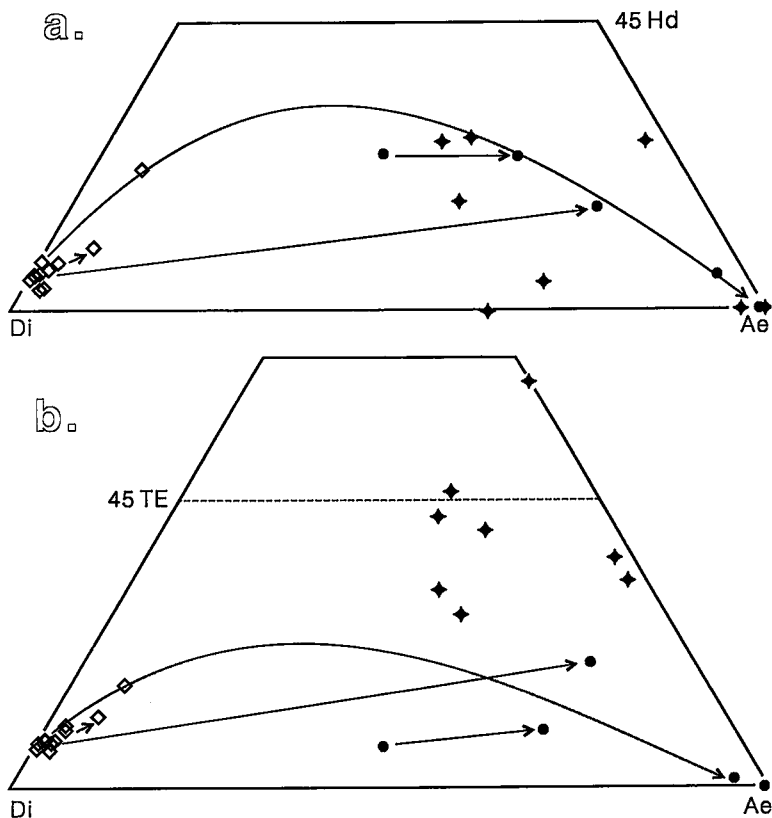


FIG. 13. Pyroxene diagrams: a. hedenbergite (Hd) – diopside (Di) – aegirine (Ae), and b.  $\text{CaMg}_{0.5}\text{Ti}_{1.5}\text{AlSiO}_6 + \text{NaFe}^{2+}_3\text{Ti}_{1.5}\text{Si}_2\text{O}_6$  (TE) – diopside (Di) – aegirine (Ae). Straight-line arrows (three for simplicity) link cores to rims, curved-line arrows indicate approximate trend during “normal” mineral development. Pyroxene colors:  $\diamond$  colorless (diopside),  $\bullet$  green (low-Ti aegirine and aegirine–augite),  $\blacklozenge$  blue-green to blue (high-Ti aegirine and aegirine–augite).

C1, C4, C5, C6, Table 6), but saturated in deep brownish green crystals (e.g., C2, C3, Table 6). A shortage of Al is common in other ferromagnesian silicates (amphiboles and micas) of the Baffin suite.

Megacrysts of colorless *pectolite* occur in dyke A (Table 6, D1). They approach a composition normal for alkaline igneous rocks, except for Mn, which is low for pectolite from this group (cf. Semenov *et al.* 1976).

#### Olivine

Phenocrysts of fresh olivine, locally approaching 10 modal %, are scattered through the marginal and internal chill-zones but, outward from these zones, the phenocrysts progressively were altered, and generally disappear within a few centimeters. Here, olivine is replaced by phlogopite (on the rims) and chlorite and

iddingsite (in the interiors). A micaceous grey pseudomorph at F has the composition

$$\text{Ca}_{0.1}[\text{Mg}_{5.1}\text{Fe}^{2+}_{0.9}]_{\Sigma=6}[\text{Si}_{7.6}\text{Al}_{0.4}]_{\Sigma=8}\text{O}_{20}[\text{OH}]_4$$

and is considered to be saponite.

The olivine is magnesium-rich. The core of phenocrysts (four dykes, N = 6) spans the narrow compositional range  $\text{Mg}^{\dagger}$  88–90. Most of these crystals are virtually unzoned, but some are enriched in Fe at a narrow rim. Notable is a phenocryst from A, where a crystal varies from  $\text{Mg}^{\dagger}$  88.7 in the core to  $\text{Mg}^{\dagger}$  79.3 at the rim; it also contains up to 0.4% MnO. The interface is poorly defined, and the rim may represent Fe-diffusion rather than primary (igneous) zonation. Nickel (0.4% NiO) is present in the core of a phenocryst from D, but was not detected at the rim and in olivine from other occurrences. The rock (area D) contains 324 ppm Ni, more than twice the amount of other specimens analyzed. Olivine grains contain 0.2–0.4%

TABLE 7. THE COMPOSITION OF TITANIUM SILICATES

No. n	<i>Shcherbakovite - batistite</i>		<i>barytolamprophyllite</i>		<i>titanite</i>	<i>lorenzenite</i>	
	TS1 1	TS2 1	TS3 1	TS4 1	TS5 3	TS6 4	TS7 7
Nb <sub>2</sub> O <sub>5</sub>	n.a.	0.51	n.a.	n.a.	n.a.	n.a.	1.40
SiO <sub>2</sub>	39.33	39.88	28.08	27.82	29.03(17)	35.90(16)	35.03
TiO <sub>2</sub>	22.00	23.94	30.24	27.70	39.84(20)	46.09(24)	45.13
Al <sub>2</sub> O <sub>3</sub>	0.12	0.07	0.46	4.61	0.07(01)	0.07(03)	n.a.
Ce <sub>2</sub> O <sub>3</sub>	n.a.	n.a.	n.a.	n.a.	0.27(10)	n.a.	n.a.
FeO	2.70	1.31	5.49	2.70	0.93(06)	0.43(04)	0.34
MnO	0.06	n.a.	1.36	0.51	<0.02	<0.02	n.a.
MgO	0.08	0.30	0.64	0.35	0.08(01)	n.a.	n.a.
CaO	1.93	0.97	1.08	0.80	27.04(30)	0.66(21)	n.a.
BaO	12.58	16.84	18.67	22.00	n.a.	0.31(12)	n.a.
Na <sub>2</sub> O	4.98	5.99	7.14	10.86	0.51(02)	17.22(03)	17.74
K <sub>2</sub> O	9.39	8.21	5.26	1.58	0.06(02)	0.08(03)	n.a.
F	0.78	n.a.	0.73	1.32	<0.10	n.a.	n.a.
Cl	<0.03	n.a.	<0.03	0.19	<0.03	n.a.	n.a.
H <sub>2</sub> O	<u>0.09</u>	<u>0.37</u>	<u>0.03</u>	<u>0.09</u>	<u>0.23</u>		
Total	93.71	98.39	98.87	99.93	98.06	100.76	99.64
<i>Cations</i>	9		12		12	12	
<i>Charge</i>	27.33	27.51	35.30	34.64	39.60	36.28	36.13
Si	4.065	4.012	3.869	3.716	3.866	4.091	4.031
Al	<u>0.000</u>	<u>0.000</u>	<u>0.075</u>	<u>0.284</u>		<u>0.000</u>	<u>0.000</u>
Σ <sub>Z</sub>	4.065	4.012	3.944	4		4.091	4.031
Nb	-----	0.023	-----	-----	-----	-----	0.073
Ti	1.710	1.811	3.134	2.782	3.991	3.950	3.905
Al	0.015	0.008	0.000	0.441	0.011	0.009	-----
Ce <sup>3+</sup>	-----	-----	-----	-----	0.013	-----	-----
Fe <sup>2+</sup>	0.233	0.110	0.633	0.302	0.104	0.041	0.033
Mn	0.005	-----	0.159	0.058	0	0	-----
Mg	<u>0.012</u>	<u>0.045</u>	0.131	0.070	0.016	-----	-----
Σ <sub>C</sub>	1.976	1.998				4.000	4.011
Ca	0.214	0.105	0.159	0.114	3.858	0.081	-----
Ba	0.509	0.664	1.008	1.151	-----	0.014	-----
Na	0.998	1.168	1.908	2.812	0.130	3.804	3.958
K	<u>1.238</u>	<u>1.054</u>	<u>0.925</u>	<u>0.269</u>	0.011	<u>0.011</u>	-----
Σ <sub>A</sub>	2.994	2.990	8.056	8		3.909	3.958

Rock types and localities: TS1 Baffin dyke at B; TS2 lamproite, Emmons Mesa, Wyoming (Mitchell & Bergman 1991); TS3 Baffin dyke at D; TS4 ijolite, Redwine River, Labrador (Singh 1972); TS5 Baffin dyke at D; TS6 Baffin dyke at E; TS7 nepheline syenite, Langedalen, Norway (Larsen *et al.* 1992). All iron is assumed divalent; H<sub>2</sub>O calculated from anion content; Σ<sub>Z</sub> includes C cations in TS3 and TS4. The proportion of the major elements, except for F and Cl, is expressed as oxides, in wt.%.

CaO, similar to those of volcanic and hypabyssal rocks in general (Simkin & Smith 1970). Chromium is close to the detection limit of the electron microprobe (*ca.* 0.02% Cr<sub>2</sub>O<sub>3</sub>).

The most distinctive feature of the olivine suite is a low silica content. All olivine grains studied are Si-depleted (<1 *apfu* Si), regardless of whether the formula is calculated with respect to cations or a fixed number of oxygen atoms. This feature is also found in olivine from lamproites elsewhere. For example, 13 of the 15 "representative compositions" in Mitchell & Bergman (1991, Table 6.28) are Si-depleted. In Table 6, the composition of zoned olivine in a Baffin dyke is compared with that of olivine from a nearby

pre-ectonic ultramafic sill analyzed by the same technique and the same data-reduction protocol.

Olivine from Sumner Island is similar in composition to olivine in the dykes at Napoleon Bay. It contains a small but significant amount of Ca (0.3% CaO), and low levels of Mn (0.1–0.2% MnO), Cr (*ca.* 0.05% Cr<sub>2</sub>O<sub>3</sub>) and Ni (<0.25% NiO).

#### MINOR MINERALS

##### *Titanium silicates*

*Shcherbakovite*, essentially <sup>4</sup>[BaK<sub>2</sub>]<sup>C</sup>Ti<sub>2</sub>Si<sub>4</sub>O<sub>14</sub>, has been described from nepheline syenite in the Kola

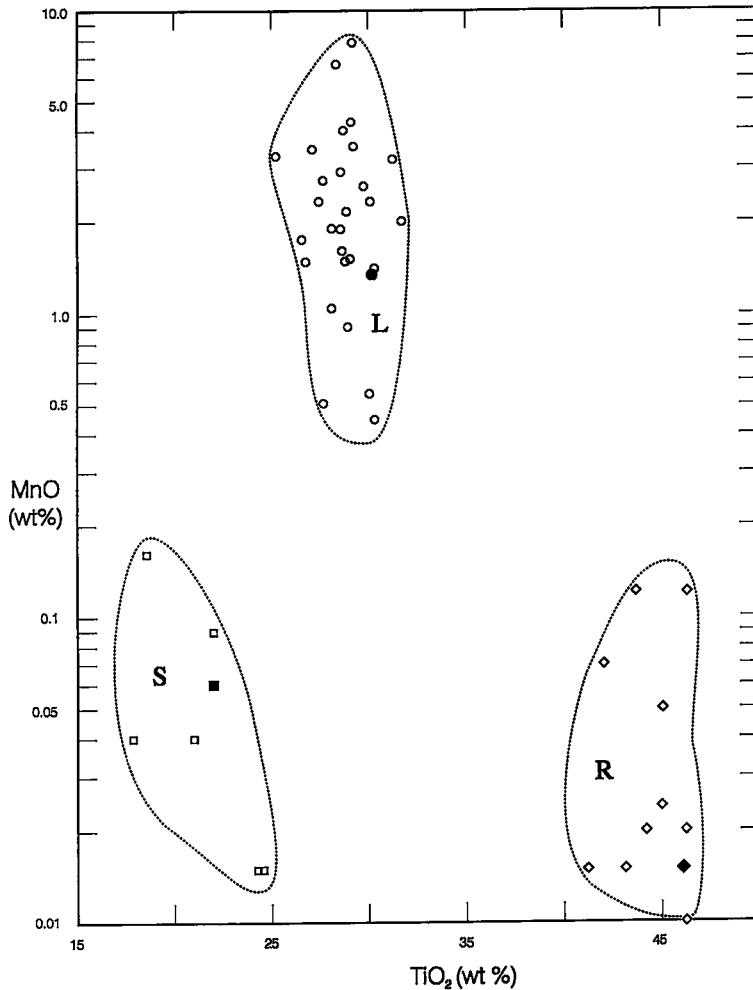


FIG. 14. Concentration of  $\text{TiO}_2$  versus that of  $\text{MnO}$  (wt%) for lamprophyllite – barytolamprophyllite (circles; L), scherbakovite–batisite (squares; S) and lorenzenite (diamonds; R). Open symbols represent compositions of minerals, worldwide, derived from the following sources: L, Pecora (1942), Semenov (1972), Singh (1972), Yakovlevskaya (1972), Kostyleva-Labuntsova *et al.* (1978), Johnsen *et al.* (1994), R.A. Gault (Mont Saint-Hilaire, unpublished); S, Kostyleva-Labuntsova *et al.* (1978), Jaques *et al.* (1986), Schmahl & Tillmanns (1987, calculated from given formula); R, Sahama (1947), Semenov (1972), Ferguson (1977, 1978), Kostyleva-Labuntsova *et al.* (“ramsayite”, 1978), Karup-Møller (1986). Solid symbols represent minerals from the Baffin dykes. Manganese ( $\text{MnO}$ ) values given as “below detection”, “not detected” and “<0.02%” have been arbitrarily assigned as 0.015%.

Peninsula, Russia (Es'kova & Kazakova 1954), peralkaline volcanic rocks at Eifel, Germany (“batisite” of Hentschel 1980, Schmahl *et al.* 1981) and lamproite from West Kimberly, Australia and Leucite Hills, Wyoming (Mitchell 1990, Mitchell & Bergman 1991). Its sodium counterpart, batisite, ideally  $\text{A}[\text{BaNa}_2]\text{C}_2\text{Ti}_2$

$\text{Si}_4\text{O}_{14}$ , has been identified from aegirine–arfvedsonite pegmatite in the Aldan Mountains, Russia, only (Kravchenko & Vlasova 1959), but “shcherbakovite” from lamproite of the Leucite Hills (Mitchell & Bergman 1991) has Na slightly dominant in A and is, therefore, just within the batisite range. Minor substitu-

tions in the shcherbakovite – batisite series include Ca for K, Nb, Mg, Fe, and Mn for Ti, Al for Si, and OH, Cl and F for O.

Tiny, round, greyish green grains occur in sanidine derived from leucite, in a Baffin dyke (area B). Analysis of the largest grain gave a low total, possibly owing to failure to determine  $\text{Nb}_2\text{O}_5$  and SrO, but its composition (Table 7, TS1) agrees well with the structural formula of Schmahl & Tillmanns (1987):  $(\text{Ba},\text{K})(\text{K},\text{Na})\text{Na}(\text{Ti},\text{Fe},\text{Al},\text{Mg},\text{Mn})_2\text{Si}_4\text{O}_{14}$ . It is here compared with the Leucite Hills batisite (Table 7, TS2).

*Barytolamprophyllite*, a minor mineral in felsic alkaline rocks, ijolite and related peralkaline pegmatites (e.g., Kostyleva-Labuntsova *et al.* 1978, Johnsen *et al.* 1994), has not been reported from lamproite. In the Baffin dykes, it is tentatively identified in a polished thin section from the southern dyke at D, where it shows extinction parallel (or approximately parallel) to a well-developed twin parting and crystal extension, positive elongation, and strong pleochroism (X' yellow, Z' brown), all properties that overlap those of phlogopite nearby. It is, however, readily distinguished from phlogopite by a much brighter BSE image and pronounced Ba peak with EDS. The grains are tiny lamellae, dispersed in sanidine in two parts of the section.

The series barytolamprophyllite  $^A[\text{NaBa}_2]_C[\text{NaFe}^{2+}\text{Ti}_3]_Z\text{Si}_4\text{O}_{18}$  – lamprophyllite  $^A[\text{NaSr}_2]_C[\text{NaFe}^{2+}\text{Ti}_3]_Z\text{Si}_4\text{O}_{18}$  is complete in nature (Peng Tze-chung & Chang Chien-hung 1965, Yakovlevskaya 1972). The mineral in the Baffin dyke (Table 7, TS3) is strongly skewed to the Ba side, although up to 1% SrO could be present locally. In addition to the elements specified in the formulae, important substitutions are evident in the literature, viz. K in A, Al,  $\text{Fe}^{3+}$ , Mn, Mg and Ca in C, Al in Z, F and OH for O. The composition of X-ray-identified barytolamprophyllite from Labrador (Table 7, TS4) is compared with that of the Baffin specimen (Table 7, TS3).

In the Baffin dykes, *titanite* can attain 2% in the mode and 0.4 mm in long diameter of crystals in the coarse-grained fraction near the dykes' center. This titanite (Table 7, TS5) has an unusually high content of alkalis, a feature that appears to characterize the mineral in alkaline and peralkaline igneous rocks. In other aspects, the composition is normal. Much of the 2% deficit in total is probably due to the presence of Nb, La, Nd and Sr (not determined). The mineral also occurs in lamproites from Western Australia (Jaques *et al.* 1986, p. 53).

*Lorenzenite*, a common accessory mineral in peralkaline syenite and granite, some cases of phonolite, and pegmatitic pockets (e.g., "ramsayite" of Kostyleva-Labuntsova *et al.* 1978, De Mark 1984, Larsen *et al.* 1992), has a composition that normally approaches  $^A\text{Na}_4^C\text{Ti}_4^Z\text{Si}_4\text{O}_{18}$ , but minor amounts of Ca, K, and Sr substitute for Na, whereas Nb, Al, Fe, Ce and Mn substitute for Ti, and F and OH for O.

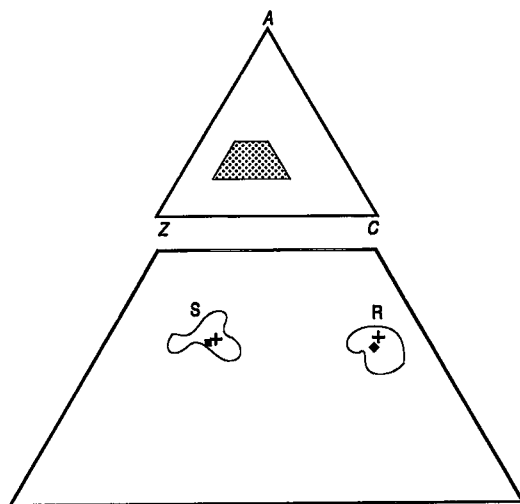


FIG. 15. ACZ plot of schcherbakovite–batisite (S) and lorenzenite (R) in alkaline and ultrapotassic rocks. Rounded areas delimit 11 compositions of S given by Prider (1965), Kostyleva-Labuntsova *et al.* (1978), Jaques *et al.* (1986), Schmahl & Tillmanns (1987), Mitchell (1990), Mitchell & Bergman (1991), and 19 compositions of R given by Sahlman (1947), Semenov (1972), Ferguson (1977, 1978), Kostyleva-Labuntsova *et al.* (1978), Karup-Møller (1986), Larsen *et al.* (1992). Ideal compositions are shown by crosses, minerals in the Baffin dykes by a solid square (S) and a diamond (R).

In the Baffin dyke at E, lorenzenite is present in fine-grained patches in the coarse fraction of the rock. Normally, the patches are zoned, with a core of lorenzenite, surrounded by two unidentified Ca–Zr silicates, a Na–Zr silicate and a Mg–Ti silicate, throughout which minute grains of  $\text{TiO}_2$  and calcio-ancylite (Ce) produce bright spots on the BSE image. Toward the edge of these patches are local concentrations of one of the Ca–Zr silicates and a K–Ti oxide. At the extreme rim are irregular accumulations of titanite.

Tiny colorless prisms of lorenzenite also occur in microveinlets that cut wallrock and parallel the contact of the dyke at area E. The veinlets are lined with fibrous "nepheline" and filled with glass. In Table 7, the composition of lorenzenite from Baffin Island (TS6) is compared with that of lorenzenite from Norway (TS7).

In the Ti silicates, Mn appears to be enriched in the order lamprophyllite – barytolamprophyllite > shcherbakovite – batisite  $\approx$  lorenzenite, and Ti, in the order lorenzenite > lamprophyllite – barytolamprophyllite > shcherbakovite – batisite (Fig. 14). Each mineral has its own domain of composition, so that, along with other data, Mn and Ti can be used to discriminate between the three groups. The composition of lorenzenite is compared with that of shcherbakovite – batisite, with respect to A, C and Z ions, in Figure 15.

TABLE 8. SELECTED COMPOSITIONS OF OXIDES

No. n	<i>Magnetite</i>		<i>chromite</i>		<i>ülvöspinel</i>		<i>ilmenite</i>		<i>Ti-Fe-K oxide</i>	
	X1	X2	X3	X4	X5	X6	X7	X8	X7	X8
	1	5	7	1	1	4	4	1	4	1
Nb <sub>2</sub> O <sub>5</sub>	n.a.	n.a.	<0.03	n.a.	<0.03	<0.03	0.36(10)	n.a.		
SiO <sub>2</sub>	<0.03	<0.03	<0.03	n.a.	<0.03	<0.03	<0.03	n.a.		
TiO <sub>2</sub>	<0.02	3.62(06)	19.85(31)	23.96	52.84	50.99(50)	80.80(75)	81.56		
Al <sub>2</sub> O <sub>3</sub>	0.19	6.30(26)	0.45(06)	0.85	0.26	<0.03	0.02(02)	0.02		
Cr <sub>2</sub> O <sub>3</sub>	0.32	48.55(67)	0.02(01)	0.11	<0.02	<0.02	0.09(06)	0.42		
V <sub>2</sub> O <sub>5</sub>	0.24	0.10(02)	0.28(04)	n.a.	0.64	0.06(02)	0.69(06)	n.a.		
Ce <sub>2</sub> O <sub>3</sub>	n.a.	n.a.	n.a.	n.a.	n.a.	n.a.	0.60(07)	n.a.		
Fe <sub>2</sub> O <sub>3</sub>	68.46	9.92(138)	30.91(65)	21.03	0.00	1.31(93)	1.35(17)	6.68		
FeO	31.20	20.55	47.45	47.76	34.47	40.89	6.17	3.50		
MnO	<0.02	0.56(18)	1.47(27)	1.40	11.76	4.52(39)	<0.02	n.a.		
ZnO	<0.02	0.10(05)	<0.02	n.a.	0.11	<0.02	n.a.	n.a.		
MgO	<0.03	9.62(82)	0.07(01)	2.26	0.23	0.17(02)	0.05(02)	n.a.		
CaO	<0.02	0.04(02)	<0.02	n.a.	0.18	0.06(05)	0.38(10)	n.a.		
BaO	n.a.	n.a.	n.a.	n.a.	n.a.	n.a.	<0.05	0.26		
K <sub>2</sub> O	n.a.	n.a.	n.a.	n.a.	n.a.	n.a.	8.91(36)	8.65		
Total	100.41	99.36	100.50	97.37	100.49	98.00	99.42	101.09		
<i>Cations</i>	24		24		4		8B			
<i>Charge</i>	64		64		12		32			
Nb	—	—	0	—	0	0	0.019	—		
Ti	0	0.740	4.376	5.444	1.988	1.973	7.145	7.046		
Al	0.069	2.020	0.163	0.303	0.015	0	0.003	0.003		
Cr	0.07	10.447	0.005	0.026	0	0	0.008	0.038		
V	0.059	0.022	0.070	—	0.026	0.003	0.065	—		
Ce	—	—	—	—	—	—	0.026	—		
Fe <sup>3+</sup>	15.795	2.031	7.010	4.782	0	0.051	0.119	0.577		
Fe <sup>2+</sup>	0	0.740	4.376	5.444	0	0	0.606	0.336		
Mg	0	0.000	0.000	0	0	0	0.009	—		
Σ <sub>B</sub>	16	16	16	16	2.03	2.03	8	8		
Fe <sup>2+</sup>	8.000	3.935	7.583	6.624	1.442	1.760	0	0		
Mn	0	0.130	0.385	0.358	0.498	0.197	0	0		
Zn	0	0.020	0	—	0.004	0	—	—		
Mg	0	3.904	0.031	1.018	0.017	0.013	0	0		
Ca	0	0.012	0	0	0.010	0.003	0.048	—		
Ba	—	—	—	—	—	—	0	0.012		
K	—	—	—	—	—	—	1.336	1.268		
Σ <sub>A</sub>	8	8	8	8	1.97	1.97	1.38	1.28		

Rock types and localities: X1 diatreme, Kodlunarn; X2, X3 Baffin dyke at B; X4 lamproite, Kapamba, Zambia (Scott Smith, in Mitchell & Bergman 1991); X5, X6 Baffin dykes at B, E; X7 Baffin dyke at F; X8 lamproite at Sisimiut, Greenland (Scott 1981). The proportion of the major elements is expressed as oxides, in wt.%.

## Oxides

Titanium-free *magnetite* occurs sparingly in diatremes at Kodlunarn and as a contact mineral in anorthosite at the Discovery Dyke. Tiny grains of chromite, ilmenite and a Ti-Fe-K oxide are distributed through the Baffin dykes and the volcanic rock at Sumner Island. An *ülvöspinel*-*ilmenite* intergrowth was observed in the Discovery Dyke. Compositions of oxide minerals from the Baffin rocks, and of similar *ülvöspinel* and Ti-Fe-K oxide, from Zambia and Greenland, respectively, are listed in Table 8.

The *ülvöspinel* - *ilmenite* intergrowth is present in the coarse-grained fraction of the dyke. Here, *ilmenite* ( $X_{\text{Hem}} = 0.111$ ; 2.3% MnO, 0.1% MgO) coexists with *ülvöspinel* ( $X_{\text{Mag}} = 0.443$ ; Table 8, anal. X3). The inter-

growth resembles the "sandwich type" of Haggerty (1991). Equilibrium conditions of the pair are  $T = 967 \pm 30^\circ\text{C}$ , at a log  $f(\text{O}_2)$  of  $11.2 \pm 0.3$  and  $\Delta\text{FMQ} + 0.07$ , using the reduction of Andersen *et al.* (1993). Thus, equilibrium was attained in the subsolidus, slightly above the oxygen fugacity of the fayalite - magnetite - quartz buffer. The texture may represent the oxidation of *ilmenite* to a magnetite phase, but the paragenetic relationship with nearby chromite is unknown. A composition (X4) of a similar spinel mineral is presented for comparison.

Small crystals of interstitial *ilmenite* (e.g., Table 8, X5 and X6) are present in all dykes. As in lamproites worldwide (Mitchell & Bergman 1991, p. 276-278), the *ilmenite* is rich in Mn (2.3 - 11.8% MnO), but poor in Cr (<0.02% Cr<sub>2</sub>O<sub>3</sub>) (Table 8, X5, X6). It differs from

ilmenite in most lamproites by the virtual absence of Mg (0.1 – 0.3% MgO), but it contains levels of Mg similar to that in ilmenite in lamproite from Sisimiut (Thy *et al.* 1987).

Spinel was observed as minute octahedra in olivine, diopside and pseudoleucite in three dykes and the Summer Island volcanic rock. It is rich in Cr (42–49% Cr<sub>2</sub>O<sub>3</sub>) and Ti (3–6% TiO<sub>2</sub>), but poor in Al (3–7% Al<sub>2</sub>O<sub>3</sub>) and Mg (2–11% MgO), resembling spinel from certain Alaskan-type peridotites (Irvine 1967, 1974), orangites (Mitchell 1995) and lamproites (Mitchell & Bergman 1991). Spinel from the Baffin suite is compared with spinel from established examples of lamproite in Figure 16, and a composition (X2) is presented in Table 8.

The Baffin spinel, chromite *sensu stricto*, resembles spinel of groups 2 and 3 of Mitchell (1985), although the composition here may not be primary. Both Fe<sup>†</sup> (Fig. 16) and Fe\* (48.7–89.0) vary considerably, with iron concentrated on the rims of crystals, suggesting that the mineral has been hydrothermally altered (Kimball 1990). This model is in accord with the vulnerability of tiny grains (<50 µm diameter) to alteration. It explains the departure of the two most Fe-rich populations from the field of spinel typical of lamproite. Nevertheless, because Cr<sup>†</sup> is relatively constant within the three rock variants, and because Fe<sup>†</sup> of chromite from an internal chill-zone overlaps Fe<sup>†</sup> of chromite from the coarse-grained interiors of the Baffin dykes, the hypothesis of secondary enrichment in iron must be regarded as tentative.

An opaque, Ba-free Ti–Fe–K oxide (Table 8, X7) occurs in dykes at A, B, E and F. It is normally anhedral, but in some cases shows rectangular sections, and in reflected light is distinctly anisotropic. This mineral appears to be similar to an oxide from lamproite at Sisimiut (Table 8, X8), syenite at Little Murun (Siberia) and orangeite in the Lace, Sover North and Star occurrences (South Africa). The composition is close to K<sub>2</sub>Ti<sub>13</sub>O<sub>27</sub> (Mitchell 1995, p. 213–216). However, its composition can also be represented by a general hollandite formula A<sub>2</sub>B<sub>8</sub>O<sub>16</sub>, calculated according to cations and charge (Table 8; X7, X8), with considerable shortfall of A cations, and Fe<sup>2+</sup> as well as Fe<sup>3+</sup> in B.

The remaining minerals are mostly distributed through the groundmass. By far the most common are fluorapatite, calcite and pyrite. Tiny, rounded grains of a mineral giving the distinctive EDS signature of *djerfisherite* (ideally, K<sub>6</sub>NaFe<sub>24</sub>S<sub>26</sub>Cl) occur in dykes at B and D (major peaks at S, K, Fe; minor peaks at Na, Cu; smaller peaks at Cl, Ni). Calcite associated with brown amphibole gives a mottled BSE image, with low BSE intensity pertaining to minor Mg (0.1% MgO), Sr (0.1% SrO) and Ba (<0.5% BaO), and relatively high BSE intensity pertaining to moderate Mg (0.5% MgO), Sr (0.5–1% SrO) and Ba (0.2–0.9% BaO). Other minerals identified by optical properties and EDS data include

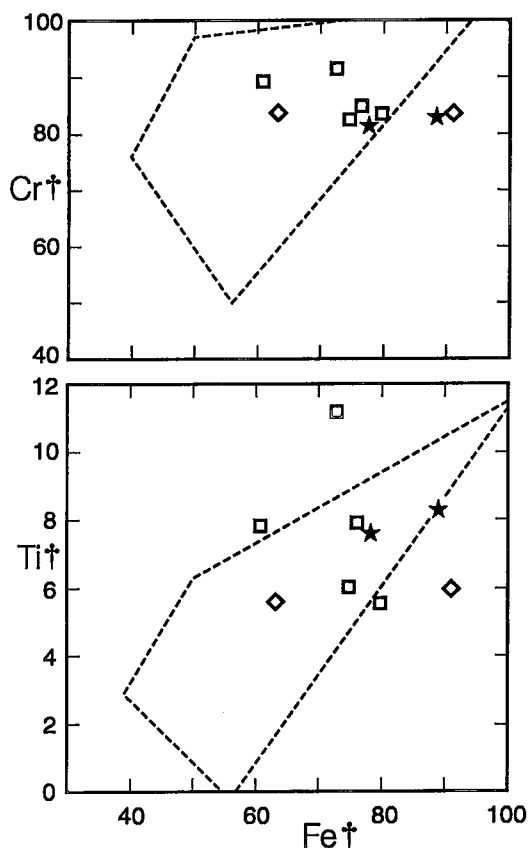


FIG. 16. Chromite diagram, with Fe<sup>†</sup> plotted against Cr<sup>†</sup> and Ti<sup>†</sup>. Broken line circumscribes the field of lamproite, which includes 18 data points taken from Mitchell (1985) and Mitchell & Bergman (1991). Symbols: ◇ crystals from an internal chill-zone of dyke, □ crystals from the coarse-grained interior, ★ crystals from Sumner Island volcanic rock.

galena, sphalerite, perovskite, pyrite, dolomite, calcio-ancylite-(Ce), strontianite, barite and zircon.

## DISCUSSION

### *Lamproites worldwide and the Baffin rocks: mineralogical similarities and differences*

Minerals in the Baffin suite support a lamproite classification. The rocks are porphyritic, with phenocrysts of phlogopite, leucite and sanidine (more rarely, olivine and clinopyroxene) in a groundmass of phlogopite, sanidine and less abundant minerals, a setting characteristic of lamproite. Most of the mineralogical criteria for lamproite listed by Mitchell & Bergman (1991,

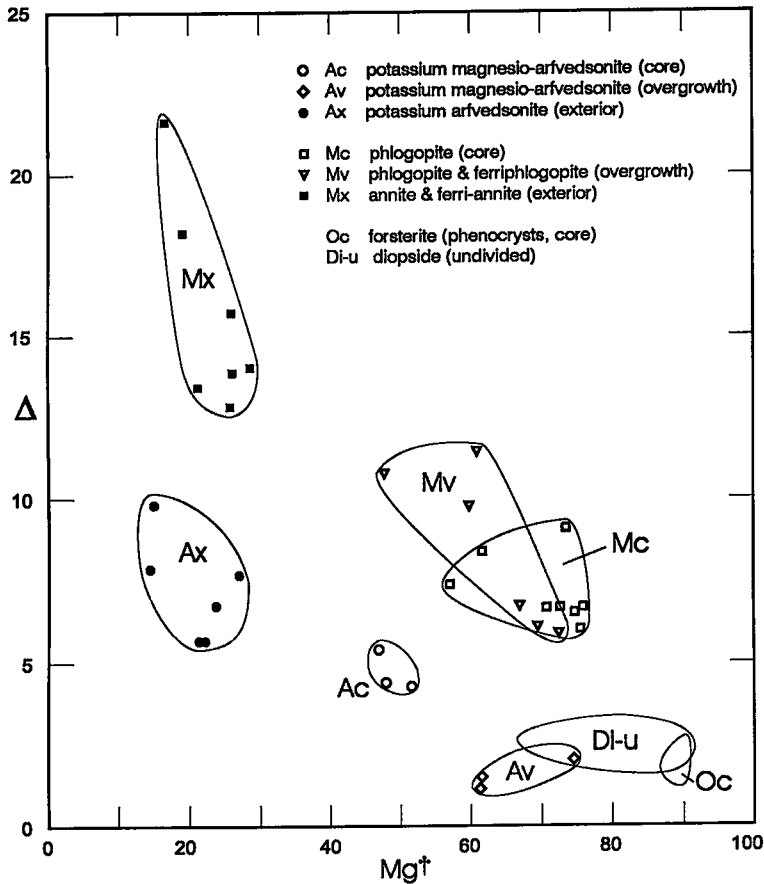


FIG. 17. Percentage deficit of Si + Al,  $\Delta$ , in the tetrahedral position versus magnesium number,  $100 \text{ Mg}/(\text{Mg} + \text{Fe}) = \text{Mg}^\dagger$ , in micas, amphiboles, diopside and olivine of the Baffin dykes. Individual plots of undifferentiated diopside (Di-u,  $N = 11$ ) and olivine cores (Oc,  $N = 6$ ) have been omitted for simplicity.

p. 37–38) are met. For example, major Ti and K in the same mineral characterize certain silicates and oxides of the Baffin suite and lamproites worldwide (e.g., amphiboles, micas and shcherbakovite), but are rare co-constituents in minerals from other environments. Other typical variants are low-Fe olivine, low-Na diopside (the most common pyroxene in the Baffin suite), Fe-rich leucite and sanidine and Ti-rich chromite. “[Tetra] ferriphlogopite” is present (though rare), but plagioclase, melilite, monticellite and garnet (all types) are absent. A nepheline-like phase appears, but only as a reaction rim at the contact with feldspathic wallrock; kalsilite is a breakdown product of leucite.

Mitchell (1985) and Mitchell & Bergman (1991) have noted that in lamproites, micas, amphiboles and pyroxenes commonly “contain insufficient aluminum [*i.e.*, Si + Al] to fill the tetrahedral sites”. In the Baffin dykes, all micas, amphiboles, forsterite and diopside are

depleted in Si +  $^{\text{IV}}\text{Al}$ . Determined as  $\Delta = 100 (Z_{\text{ideal}} - \text{Si} - ^{\text{IV}}\text{Al})/Z_{\text{ideal}}$ , these minerals give the following average compositions, listed in descending order of tetrahedral-site deficit: titanian annite and ferri-annite margins 15.7 (3.2)%,  $N = 7$ , titanian phlogopite and “ferriphlogopite” overgrowths 8.4 (2.5)%,  $N = 6$ , titanian phlogopite cores 7.2 (1.0)%,  $N = 8$ , potassium arfvedsonite margins 7.2 (1.6)%,  $N = 6$ , potassium magnesio-arfvedsonite cores 4.7 (0.6)%,  $N = 3$ , diopside cores 2.4 (0.4),  $N = 11$ , forsterite cores 1.8(0.3),  $N = 6$ , potassium magnesio-arfvedsonite overgrowths 1.5 (0.4),  $N = 3$ . Mineral groups show a tendency for tetrahedral-site vacancies to increase with decreasing magnesium number (Fig. 17), but aegirine and aegirine-augite are within the limits of error.

Certain minor minerals in the Baffin dykes have not been heretofore described from lamproite. New are pectolite, barytolamprophyllite, calcio-ancylite-(Ce) and

TABLE 9. COMPARISON OF LAMPROITE FROM SISIMIUT AND NAPOLEON BAY

Feature	Sisimiut	Napoleon Bay
Phlogopite age(s)	1240 ± 130, 1227 ± 12 my. (K/Ar)	1240 ± 9, (K/Ar)
Intrusives	narrow dykes	narrow dykes
Disposition of dykes	E-W to NW-SE, vertical	E-W to NW-SE, vertical
Chill zones	marginal and internal	marginal and internal
Late features of dykes	reopening, carbonatization	reopening, carbonatization
Dyke texture	porphyritic	porphyritic
Phenocrysts	phlogopite, pseudoleucite, olivine, diopside most common	phlogopite, pseudoleucite, olivine, diopside most common
Olivine	forsterite, fo 87-93, ave Δ=0	forsterite, fo 80-92, ave Δ=1.8%
Early pyroxene	diopside, 0.2-1.9% TiO <sub>2</sub> , 0.2-1.0% Al <sub>2</sub> O <sub>3</sub> , ave Δ=1.0	diopside, <0.02-2.3% TiO <sub>2</sub> , 0.6-1.3% Al <sub>2</sub> O <sub>3</sub> , ave Δ=2.4
Amphibole	normally K-rich, alkali amphiboles common, Na-Ca amphiboles less common, ave Δ=2.2	normally K-rich, alkali amphiboles common, Na-Ca amphiboles less common, ave Δ=4.5
Phlogopite	iron enrichment on margin, 2.8 - 10.3% TiO <sub>2</sub> , ave Δ=7.4	iron enrichment on margin, 2.9 - 9.0 % TiO <sub>2</sub> , ave Δ=11.4
Overgrowths on mica	"ferriphlogopite", 19.4-20.0% MgO, ave Δ=16.9	"ferriphlogopite" and phlogopite, 12.2 - 19.3% MgO, ave Δ=8.4
Leucite, <i>sensu stricto</i>	rare, in marginal chill zone only	rare, in internal chill zone only
Pseudoleucite	common	common (sanidine + kalsilite)
Sanidine	common, 0.1 - 3.8% Fe <sub>2</sub> O <sub>3</sub>	common, 0.1 - 1.6% Fe <sub>2</sub> O <sub>3</sub>
Carbonate	calcite locally common	calcite locally common

Sources: *Sisimiut* - Brooks *et al.* (1978), Larsen *et al.* (1983), Scott (1977, 1981), Thy (1982), Thy *et al.* (1987), Winter (1974); *Napoleon Bay* - Geol. Surv. Canada. (unpublished K/Ar age).

lorenzenite, minerals characteristic of peralkaline intrusive suites, and djerfisherite, a phase noted in peridotites, kimberlites, and chondritic meteorites. Rather different from most lamproites are the high alkali and iron contents of some minerals in the dykes. Potassium arfvedsonite, annite and aegirine are not characteristic of lamproite, though each has been reported.

The diatremes on Kodlunarn, choked with xenoliths but cemented with peraluminous and high-potassium glass, are provisionally placed in this volcanogenic suite and considered to be a forerunner of the Baffin dykes. This coupling is made by analogy to other lamproites, where an early explosive facies is present in the majority of occurrences (Mitchell & Bergman 1991, p. 137-157). Glass in Precambrian rocks requires special conditions for preservation, and is rare. Another model, which cannot be summarily dismissed, states that the diatreme dykes may be manifestations of Cenozoic volcanism, which includes extrusion of basalt as

part of the Tertiary north Atlantic volcanic province, on the coast of Baffin Island, 450 km NNE (Clarke & Upton 1971).

Of the various ultrapotassic rocks described to date, the Baffin dykes correspond most closely to lamproites near Sisimiut, in west Greenland. This similarity is summarized in Table 9. The Sisimiut lamproites are 700 km northeast of Napoleon Bay, and the correspondence of dyke trends suggests a post-intrusive separation of Baffin Island from Greenland in a sinistral sense, without rotation.

Lamproites are generally restricted to mobile belts surrounding continental cratons (Mitchell & Bergman 1991, p. 406). The Baffin and Sisimiut dykes, lying at the edge of the North American craton, fit admirably into this framework. As with many other occurrences, the lamproites were not emplaced until tensional fractures permitted introduction of subcrustal melts, long after the last deformation had ceased.

## CONCLUSIONS

Mineral development in the Baffin suite can be summarized, tentatively, in the following stages:

1) Intrusion of diatreme dykes and sills. Cementation with peraluminous, K-rich glass (Kodlunarn Island).

2) Emplacement of lamproite dykes (Napoleon Bay) and lamproite flows (source of the Sumner Island cobble). Characteristic minerals: forsterite, phlogopite-annite, diopside, leucite, sanidine. Late-stage alkali amphiboles. Main chemical trends of micas and amphiboles: Fe-enrichment, and depletion in Si, Al, and F.

3) Cooling, solidification and fracturing of lamproite dykes.

4) Introduction of new material along fractures. Characteristic minerals: overgrowths of aegirine and aegirine-augite, phlogopite and "ferriphlogopite", magnesio-arfvedsonite. Compositional trends of pyroxene: enrichment in Na, Fe. Possibly, pectolite belongs to this generation. Calcite postdates magnesio-arfvedsonite.

5) Post-consolidation effects: phase inversion and exsolution of leucite; oxidation of ilmenite.

The chemical evolution of minerals during stage 2 is an extreme example of magmatic differentiation, but the abrupt change from stage 2 to 4 requires an overhaul of the system and presents a special problem. Stage 4 may represent postmagmatic, hydrothermal development, although very sharp zoning in some amphibole crystals favors magma mixing and introduction of an H<sub>2</sub>O-saturated silicate melt. However, amphibole-lined cavities, filled with low- to moderate-Mg, low- to moderate-Sr calcite, imply late-stage circulation of hydrothermal, CO<sub>2</sub>-rich fluid. That Precambrian glass survives in the contact zone implies the melt was quenched and was not followed by later introduction of H<sub>2</sub>O or by a thermal event.

## ACKNOWLEDGEMENTS

Thanks are due to the following persons for contributions to this research: Bill Fitzhugh (Smithsonian Institution) and Reg Auger (Université Laval) for including the author in their field parties of 1992 and 1994; André Gonciar and Paulusie Pishuktie for field assistance; Scott Ercit, Glenn Poirier and Peter Jones for help with electron-microprobe analyses; George Rossman and Barbara Scott-Smith for valuable discussions; Roger Mitchell and Steve Bergman for writing the definitive text on lamproites, which facilitated comparisons and from which many ideas in this paper are based. Helpful comments by Dan Barker (referee), Keith Bell, Steve Bergman (referee), Nelson Eby, Tony Fowler, Bob Martin and Tony Peterson greatly improved the manuscript. Hélène DeGouffe and Sylvie Downing typed the manuscript. Computer drawings were made by Edward Hearn.

## REFERENCES

- ABU-EID, R.M. (1976): Absorption spectra of transitional metal-bearing minerals at high pressures. *In* The Physics and Chemistry of Minerals and Rocks (R.G.J. Strens, ed.). Wiley, London, U.K. (327-346).
- ANDERSEN, D.J., LINDSLEY, D.H. & DAVIDSON, P.M. (1993): QUILF: a PASCAL program to assess equilibria among Fe-Mg-Mn-Ti oxides, pyroxenes, olivine and quartz. *Comput. Geosci.* **19**, 1333-1350.
- BLACKADAR, R.G. (1967): Geological reconnaissance, southern Baffin Island, District of Franklin. *Geol. Surv. Can., Pap.* **66-47**.
- BROOKS, C.K., NOE-NYGAARD, A., REX, D.C. & RØNSBO, J.G. (1978): An occurrence of ultrapotassic dikes in the neighbourhood of Holsteinsborg, west Greenland. *Bull. Geol. Soc. Denmark* **27**, 1-8.
- CLARKE, D.B. & UPTON, B.G.J. (1971): Tertiary basalts of Baffin Island: field relations and tectonic setting. *Can. J. Earth Sci.* **8**, 248-258.
- CUNDARI, A. (1973): Petrology of the leucite-bearing lavas in New South Wales. *J. Geol. Soc. Australia* **20**, 465-492.
- CURTIS, L.W. & GITTINS, J. (1979): Aluminous and titaniferous clinopyroxenes from regionally metamorphosed agpaite rocks in central Labrador. *J. Petrol.* **20**, 165-186.
- DE MARK, R.S. (1984): Minerals of Point of Rocks, New Mexico. *Mineral. Rec.* **15**, 150-156.
- ESKOVA, E.M. & KAZAKOVA, M.E. (1954): Shcherbakovite - a new mineral. *Dokl. Akad. Nauk SSSR* **99**, 837-841 (in Russ.). Abstr. in *Am. Mineral.* **40**, 788.
- FERGUSON, A.K. (1977): Note on a ramsayite-bearing pegmatoidal clot in a mela-nephelinite from the older volcanics near Bacchus Marsh, Victoria. *J. Geol. Soc. Aust.* **24**, 491-494.
- \_\_\_\_\_ (1978): The occurrence of ramsayite, titan-lâvenite and fluorine-rich euclite in a nepheline-syenite inclusion from Tenerife, Canary Islands. *Contrib. Mineral. Petrol.* **66**, 15-20.
- GITTINS, J., FAWCETT, J.J., BROOKS, C.K. & RUCKLIDGE, J.C. (1980): Intergrowths of nepheline - potassium feldspar and kalsilite - potassium feldspar: a re-examination of the 'pseudo-leucite problem'. *Contrib. Mineral. Petrol.* **73**, 119-126.
- GONNARD, F. (1909): Sur les groupements cristallins de l'olivine de Maillargues (Cantal). *Bull. Soc. fr. Minéral.* **32**, 81-82.
- HAGGERTY, S.E. (1991): Oxide textures - a mini-atlas. *Rev. Mineral.* **25**, 129-219.
- HENTSCHEL, G. (1980): Weitere bemerkenswerte Mineralfunde aus quartären Vulkanvorkommen der Eifel. *Mainzer geowiss. Mitt.* **6**, 169-172.

- HOGARTH, D.D., BOREHAM, P.W. & MITCHELL, J.G. (1994): Martin Frobisher's northwest venture: mines, minerals and metallurgy. *Can. Museum Civilization, Mercury Ser., Directorate Pap.* 7.
- \_\_\_\_\_ & GIBBINS, W.A. (1984): Martin Frobisher's gold mines on Kodlunarn Island and adjacent Baffin Island, Frobisher Bay, NWT. *Contrib. Geol. Northwest Territories* 1, 69-78.
- \_\_\_\_\_ & PETERSON, T.D. (1996): Lamproite dykes of southeast Baffin Island. In *Searching for Diamonds in Canada* (A.N. LeCheminant, D.G. Richardson, R.N.W. DiLabio & K.A. Richardson, eds.). *Geol. Surv. Can., Open-File Rep.* 3228, 109-110.
- \_\_\_\_\_ & RODDICK, J.C. (1989): Discovery of Martin Frobisher's Baffin Island "ore" in Ireland. *Can. J. Earth Sci.* 26, 1053-1060.
- IRVINE, T.N. (1967): Chromian spinel as a petrogenic indicator. 2. Petrologic applications. *Can. J. Earth Sci.* 4, 71-103.
- \_\_\_\_\_ (1974): Petrology of the Duke Island ultramafic complex, southeastern Alaska. *Geol. Soc. Am., Mem.* 138.
- JACKSON, G.D., HUNT, P.A., LOVERIDGE, W.D. & PARRISH, R.R. (1990): Reconnaissance geochronology of Baffin Island, N.W.T. *Geol. Surv. Can., Pap.* 89-2, 123-148.
- \_\_\_\_\_ & MORGAN, W.C. (1978): Precambrian metamorphism on Baffin and Bylot Islands. *Geol. Surv. Can., Pap.* 78-10, 249-267.
- JAQUES, A.L., LEWIS, J.D. & SMITH, C.B. (1986): The kimberlites and lamproites of Western Australia. *Geol. Surv. W. Aust., Bull.* 132.
- JOHNSEN, O., NIELSEN, T.F.D. & RØNSBO, J.G. (1994): Lamprophyllite and barytolamprophyllite from the Tertiary Gardiner Complex, east Greenland. *Neues Jahrb. Mineral., Monash.*, 328-336.
- KARUP-MØLLER, S. (1986): Murmanite from the Ilímaussaq alkaline complex, south Greenland. *Neues Jahrb. Mineral., Abh.* 155, 67-88.
- KIMBALL, K.L. (1990): Effects of hydrothermal alteration on the compositions of chromian spinels. *Contrib. Mineral. Petrol.* 105, 337-346.
- KOSTYLEVA-LABUNTSOVA, E.E., BARUTSKII, B.E., SOKOLOVA, M.N., SLYUKOVA, Z.V., DORFMAN, M.D., DUDKIN, O.B., KOZIREVA, L.B. & IKORSKII, C.V. (1978): Mineralogy of the Khibina Massif (F.V. Chukhrov, ed.) 2. Nauka Press, Moscow, Russia (in Russ.).
- KRAVCHENKO, S.M. & VLASOVA, E.V. (1959): Rare metal mineralization associated with nepheline syenites of the alkaline province of central Aldan. *Dokl. Akad. Nauk SSSR* 128, 1046-1049 (in Russ.; abstr. in *Mineral. Abstr.* 15, 361).
- KRETZ, R. (1983): Symbols for rock-forming minerals. *Am. Mineral.* 68, 277-279.
- LARSEN, A.O., RAADE, G. & SÆBØ, P.C. (1992): Lorenzenite from the Bratthagen nepheline syenite pegmatites, Lågendalen, Oslo region, Norway. *Norsk Geol. Tidsskr.* 72, 381-384.
- LARSEN, L.M., REX, D.C. & SECHER, K. (1983): The age of carbonatites, kimberlites, and lamprophyres from southern west Greenland: recurrent alkaline magmatism during 2500 million years. *Lithos* 16, 215-221.
- LEAKE, B.E. (1978): Nomenclature of amphiboles. *Can. Mineral.* 16, 501-520.
- MCCORMICK, G. & LE BAS, M.J. (1996): Phlogopite crystallization in carbonatitic magmas from Uganda. *Can. Mineral.* 34, 469-478.
- MITCHELL, R.H. (1985): A review of the mineralogy of lamproites. *Trans. Geol. Soc. S. Afr.* 88, 411-437.
- \_\_\_\_\_ (1990): Shcherbakovite in leucite phlogopite lamproites from the Leucite Hills, Wyoming. *Mineral. Mag.* 54, 645-646.
- \_\_\_\_\_ (1995): *Kimberlites, Orangeites, and Related Rocks*. Plenum Press, New York, N.Y.
- \_\_\_\_\_ & BERGMAN, S.C. (1991): *Petrology of Lamproites*. Plenum Press, New York, N.Y.
- MIYANO, T. & MIYANO, S. (1982): Ferri-annite from the Dales Gorge Member iron-formations, Wittenoom area, Western Australia. *Am. Mineral.* 67, 1179-1194.
- MORIMOTO, N. (1989): Nomenclature of pyroxenes. *Can. Mineral.* 27, 143-156.
- NICKEL, E.H. (1992): Nomenclature for mineral solid solutions. *Am. Mineral.* 77, 660-662.
- \_\_\_\_\_ & NICHOLS, M.C. (1991): *Mineral Reference Manual*. Van Nostrand Reinhold, New York, N.Y.
- OBERTI, R., UNGARETTI, L., CANNILLO, E. & HAWTHORNE, F.C. (1992): The behaviour of Ti in amphiboles. I. Four- and six-coordinate Ti in richterite. *Eur. J. Mineral.* 4, 425-439.
- PECORA, W.T. (1942): Nepheline syenite pegmatites, Rocky Boy Stock, Bearpaw Mountains, Montana. *Am. Mineral.* 27, 397-424.
- PENG TZE-CHUNG & CHANG CHIEN-HUNG (1965): New varieties of lamprophyllite - barytolamprophyllite and orthorhombic lamprophyllite. *Scientia Sinica* 14, 1827-1840.
- PRIDER, R.T. (1965): Noonkanbahite, a potassic batisite from the lamproites of Western Australia. *Mineral. Mag.* 34, 403-405.
- RIMSKAYA-KORSAKOVA, O.M. & SOKOLOVA, E.P. (1964): On iron-magnesium mica with a reversed absorption scheme. *Zap. Vses. Mineralog. Obshchest.* 93, 411-423 (in Russ.).
- ROSSMAN, G.R. (1984): Spectroscopy of micas. In *Micas* (S.W. Bailey, ed.). *Rev. Mineral.* 13, 145-181.

- SAHAMA, T.G. (1947): Analysis of ramsayite and lorenzenite. *Am. Mineral.* **32**, 59-63.
- SCARFE, C.M., LUTH, W.C. & TUTTLE, O.F. (1966): An experimental study on the absence of leucite in plutonic rocks. *Am. Mineral.* **51**, 726-735.
- SCHMAHL, W.W. & TILLMANN, E. (1987): Isomorphic substitutions, straight Si-O-Si geometry, and disorder of tetrahedral tilting in batisite, (Ba, K) (K, Na) Na (Ti, Fe, Nb, Zr) Si<sub>4</sub>O<sub>14</sub>. *Neues Jahrb. Mineral., Monatsh.*, 107-118.
- \_\_\_\_\_, \_\_\_\_\_ & ABRAHAM, K. (1981): Struktur und Kristallchemie von Batisit aus der Westeifel. *Fortschr. Mineral.* **59**(1), 174-176.
- SCOTT, B.H. (1977): *Petrogenesis of Kimberlites and Associated Potassic Lamprophyres from Central West Greenland*. Ph.D. thesis, Univ. Edinburgh, Edinburgh, U.K.
- \_\_\_\_\_. (1981): Kimberlite and lamproite dykes from Holsteinsborg, west Greenland. *Medd. om Grønland, Geosci.* **4**, 1-24.
- SCOTT, D.J. (1996): Geology of the Hall Peninsula, east of Iqaluit, southern Baffin Island, Northwest Territories. *Geol. Surv. Can., Current Res.* **1996C**, 83-91.
- SEMENOV, E.I. (1972): *Mineralogy of the Lovozero Alkaline Massif*. Nauka Press, Moscow, Russia (in Russ.).
- \_\_\_\_\_, MAKSIMYUK, I.E. & ARKANGELSKAYA, V.N. (1976): On minerals of the pectolite - serandite group. *Zap. Vses. Mineral. Obshchest.* **104**, 154-163 (in Russ.).
- SIMKIN, T. & SMITH, J.V. (1970): Minor element distribution in olivine. *J. Geol.* **78**, 304-325.
- SINGH, S.K. (1972): *Petrological and Mineralogical Studies of the Joan Lake Alkalic Complex, Central Labrador*. Ph.D. thesis, Univ. Ottawa, Ottawa, Ontario.
- STRENS, R.G.J., MAO, H.K. & BELL, P.M. (1982): Quantitative spectra and optics of some meteoritic and terrestrial clinopyroxenes. In *Advances in Physical Geochemistry 2* (S.K. Saxena, ed.). Springer-Verlag, New York, N.Y. (327-346).
- THY, P. (1982): Richterite - arfvedsonite - riebeckite - actinolite assemblage from MARID dikes associated with ultrapotassic magmatic activity in central west Greenland. *Terra Cognita* **2**, 247-249.
- \_\_\_\_\_, STECHER, O. & KORSTGÅRD, J.A. (1987): Mineral chemistry and crystallization sequences in kimberlite and lamproite dikes from the Sisimiut area, central west Greenland. *Lithos* **20**, 391-417.
- VERES, G.I., MERENKOVA, T.B. & OSTROVSKII, I.A. (1955): Synthetic iron hydroxyl mica. *Dokl. Akad. Nauk SSSR* **101**, 147-150 (in Russ.).
- WINTER, J. (1974): The Precambrian geology of the Túngarnit nunâf area, outer Nordre Strømfjord, central west Greenland. *Rapp. Grøn. Geol. Unders.* **61**.
- WONES, D.R. (1963): Phase equilibria of "ferriannite", KFe<sup>2+</sup><sub>3</sub>Fe<sub>3</sub>Si<sub>3</sub>O<sub>10</sub>(OH)<sub>2</sub>. *Am. J. Sci.* **261**, 581-596.
- YAKOVLEVSKAYA, T.A. (1972): Lamprophyllite, barytolamprophyllite. In *Minerals 3*(1) (F.V. Chukhrov, ed.). Nauka Press, Moscow, Russia (in Russ.; 638-645).

Received May 25, 1996, revised manuscript accepted November 11, 1996.